HHS Public Access

Author manuscript

Sci Immunol. Author manuscript; available in PMC 2024 February 01.

Published in final edited form as:

Sci Immunol. 2023 November 03; 8(89): eadi8217. doi:10.1126/sciimmunol.adi8217.

Distinct use of super-enhancer elements controls cell-type specific CD25 transcription and function

Rosanne Spolski[1,†], **Peng Li**[1,†], **Vivek Chandra**[2], **Boyoung Shin**[3], **Shubham Goel**[4], **Keiko Sakamoto**[4,5], **Chengyu Liu**[1], **Jangsuk Oh**[1], **Min Ren**[1], **Yutaka Enomoto**[1], **Erin E. West**[1], **Stephen M. Christensen**[1], **Edwin C.K. Wan**[1], **Meili Ge**[1], **Jian-Xin Lin**[1], **Bingyu Yan**[6], **Majid Kazemian**[6], **Zu-Xi Yu**[7], **Keisuke Nagao**[4], **Pandurangan Vijayanand**[2], **Ellen V. Rothenberg**[3], **Warren J. Leonard**[1]

[1]Laboratory of Molecular Immunology, Immunology Center, National Heart, Lung and Blood Institute, National Institutes of Health, Bethesda, MD 20892-1674

[2]La Jolla Institute for Immunology, La Jolla, CA

[3]Division of Biology and Biological Engineering, California Institute of Technology, Pasadena, CA

[4]Cutaneous Leukocyte Biology Section, Dermatology Branch, National Institute of Arthritis and Musculoskeletal and Skin Diseases, National Institutes of Health, Bethesda, MD 20892

[5]Hamamatsu University School of Medicine, Department of Dermatology, Hamamatsu, Japan

[6]Department of Biochemistry, Purdue University, West Lafayette, IN

[7]Pathology Core, National Heart, Lung, and Blood Institute, National Institutes of Health, Bethesda, MD 20892

Abstract

The IL-2 receptor α-chain (IL-2Rα/CD25) is constitutively expressed on double negative (DN 2/DN3 thymocytes and regulatory T cells (Tregs) but induced by IL-2 on T and natural killer (NK) cells, with *Il2ra* expression regulated by a STAT5-dependent super-enhancer. Here, we

E.C.K.W., Department of Microbiology, Immunology, and Cell Biology, West Virginia University, Morgantown, WV 26506
M.G., State Key Laboratory of Experimental Hematology, Institute of Hematology & Blood Diseases Hospital, Chinese Academy of Medical Sciences & Peking Union Medical College,
Tianjin 300020, People's Republic of China.
Y.E., Molecular Pharmacology of Malignant Diseases, Graduate School of Pharmaceutical Sciences, The University of Tokyo, Tokyo, Japan.
[†]These authors contributed equally.

Author Contributions: R.S. and P.L. designed the project, performed experiments, interpreted data, and wrote the manuscript. V.C. and P.V performed HiChIP experiments and analyzed the data. P.L and S.M.C. performed computational analysis. B.S. and E.V.R. performed the DN thymocyte in vitro experiments and ChIP-Seq experiments and analyzed data and wrote the manuscript. S.G, K.S., and K.N. performed the experiments on alopecia skin and analyzed the data. Z.Y. performed the histological analysis of alopecia. C.L. and J.O. designed and constructed mouse deletion mutants. M.R, Y.E, E.E.W., E.W., J.O., M.G., and J.L. contributed to in vitro cloning, animal experiments, and ChIP-Seq experiments. W.J.L. supervised the project and wrote the manuscript.

List of Supplementary Materials:
Materials and Methods
Fig. S1–S9.
Table S1–S6.
Data file S1.
MDAR Reproducibility Checklist.

Competing interests: The authors declare that they have no competing interests.

investigated CD25 regulation and function using a series of mice with deletions spanning STAT5-binding elements. Deleting the upstream super-enhancer region mainly affected constitutive CD25 expression on DN2/DN3 thymocytes and Tregs, with these mice developing autoimmune alopecia, whereas deleting an intronic region decreased IL-2-induced CD25 on peripheral T and NK cells. Thus, distinct super-enhancer elements preferentially control constitutive versus inducible expression in a cell-type-specific manner. Interestingly, the Mediator-1 coactivator co-localized with specific STAT5-binding sites. Moreover, both upstream and intronic regions had extensive chromatin interactions, and deletion of either region altered the super-enhancer structure in mature T cells. These results demonstrate differential functions for distinct super-enhancer elements, thereby indicating previously unknown ways to manipulate CD25 expression in a cell-type specific fashion.

One Sentence Summary:

Distinctive *Il2ra* super-enhancer element usage in different lineages indicates how to control cell-type specific CD25 expression.

Introduction

Super-enhancers are extended regions of chromatin that bind transcription factors and coactivators at high density and orchestrate the formation of nuclear condensates, which drives transcription of key genes involved in lineage establishment or maintenance (1, 2). Super-enhancers are variably considered to represent distinctive structures or to be comprised of multiple individual typical enhancers (1, 3, 4), and they are dynamic structures that can be remodeled during differentiation or in response to external signals (5), with context-dependent roles. Coactivators such as Mediator complex subunit 1 (MED1) and Bromodomain protein 4 (BRD4) can form phase-separated condensates at super-enhancers, thereby concentrating the transcription apparatus at key cell-identity genes and influencing their expression. Moreover, studies of super-enhancers have provided insights into the mechanisms underlying gene control in normal and pathologic states (6, 7). Super-enhancer activity can be modulated by 3-dimensional chromatin interactions organized into compartments denoted as topologically-associating domains (TADs) (8).

The human and mouse genes encoding IL-2Rα (CD25) have been extensively studied over the years to explain the responsiveness of this gene to activation both via the T cell receptor and IL-2. Our lab and others identified a series of upstream positive regulatory regions (PRRs), including PRRI, PRRII, PRRIII, where PRRI and PRRII were required for the mitogenic induction of the *IL2RA* gene and PRRIII was an IL-2 response element, as well as a CD28 response element (9–18). PRRIII bound STAT5A and STAT5B proteins as well as ELF-1, HMG-I(Y), and a GATA-1-like protein. Our lab then characterized another IL-2-regulated element, PRRIV, that could bind STAT5 proteins and HMG-I(Y) (19, 20). We subsequently showed that the *Il2ra* super-enhancer is the top-ranked IL-2/STAT5-dependent super-enhancer in mouse pre-activated T cells, comprising approximately 13 STAT5 binding sites and exhibiting potent activity upon IL-2 stimulation (21). The corresponding super-enhancer in the human *IL2RA* locus has a similar overall organization (21). We previously deleted three individual STAT5 binding sites (one upstream and two intronic) in mice

using CRISPR/Cas9 technology and showed that each deletion partially contributed to IL-2-induced *Il2ra* expression in mature $CD8^+$ T cells. Moreover, the mutation in mice of an autoimmunity risk variant in an intronic enhancer delayed but did not abrogate *Il2ra* gene expression upon TCR stimulation in mature T cells (22). However, it is not clear how individual super-enhancer elements throughout the gene contribute to cell-type specific *Il2ra* expression during development, in different lineages, and in response to stimuli.

To further understand *Il2ra* regulation, here we have generated a range of individual or combinatory deletions of STAT5-bound regulatory elements in the *Il2ra* super-enhancer *in vivo* and analyzed their functions in multiple cell types, including in response to cytokine stimulation. CD25 expression varies at different stages of mouse lymphoid development. It is constitutively expressed in subsets of double negative (DN) thymocytes (DN2/DN3) and in regulatory T cells (Treg cells); by contrast, CD25 is not expressed in resting T or NK cells but is induced in response to appropriate antigen or cytokine signals (20, 23). We show that STAT5 is important for normal CD25 expression at specific DN stages of T cell development as well as in mature $CD8^+$ T cells. We reasoned that focusing on the STAT5 binding sites would allow us to identify important enhancer elements that regulate expression during development or in response to T cell receptor or cytokine signals. Strikingly, we found that distinct super-enhancer regions preferentially control constitutive versus inducible CD25 expression at different stages of T cell development and in other cell types as well, with development of spontaneous autoimmune alopecia in mice lacking the upstream super-enhancer region, correlating with defective Treg cells in these animals. Furthermore, we show extensive looping within this super-enhancer, with intronic regions dominantly affecting the overall chromatin structure and activity of the gene in mature lymphocytes, and moreover, we show the co-localization of the MED1 coactivator and of transcription factors NFATc1, FOXP3, TCF1, and SMAD4 at the super-enhancer. This detailed analysis provides mechanistic insights into CD25 regulation not only by IL-2 but also by TCR and TGFβ signals throughout early T cell development as well as in specific functional T cell subsets.

Results

Lineage- and developmental-specific STAT5 binding and open chromatin structure at the *Il2ra* locus.

We initially examined the STAT5 binding profile at the *Il2ra* locus in multiple immune cell populations using ChIP-Seq (Fig. 1A; the top enriched STAT5-binding GAS (gamma-activated sequence) motifs in each cell type are shown in Table S1, and the GAS motif at each upstream and intronic site is shown in Table S2). TCR-activated $CD8^+$ T cells and inducible Treg (iTreg) cells had similar STAT5 binding profiles in response to IL-2 stimulation, with most of the upstream and intronic sites occupied, whereas little STAT5 binding was observed in these cells in the absence of IL-2 stimulation (Fig. 1A). Distinctive STAT5 binding patterns were found in natural Treg cells isolated ex vivo, as well as in natural killer (NK) cells stimulated with IL-15, splenic dendritic cells (DCs) stimulated with GM-CSF, and in mast cells stimulated with anti-IgE (Fig. 1A), suggesting that distinct *Il2ra* super-enhancer elements might be differentially utilized in a cell-type-specific fashion.

During early mouse T cell development, CD25 is a key marker of DN thymocytes that is expressed in the DN2 and DN3 stages bridging T-cell lineage commitment (24). Although *Stat5a* and *Stat5b* deletion severely compromises early T cell development (25), and in the individual absence of either *Stat5a* or *Stat5b*, there is a partial defect in T cell numbers and/or in IL-2-induced CD25 expression (26, 27), it remains unclear whether CD25 expression in DN thymocytes is dependent on STAT5 activation and binding to the *Il2ra* gene. To investigate this, we first identified the stage at which STAT5 is activated by IL-7. By testing the impact of IL-7 exposure on freshly purified DN thymocyte subsets (fig. S1, A and B), we found that the STAT5 phosphorylation (pYSTAT5) response appeared sharply in the DN thymocytes that first express CD25, namely in DN2a and DN2b cells, then extended into DN3 cells but shut off in DN4 cells (fig. S1, C and D; a *Bcl11b-mCitrine* reporter gene was also present as a precise landmark for T lineage commitment). Next, we used sgRNAs to acutely delete both *Stat5a* and *Stat5b* in normal Cas9;*Bcl2*-transgenic hematopoietic precursors, starting one stage before CD25 is normally expressed, and we examined the effects of STAT5 loss on early T-lineage development in artificial thymic organoid (ATO) (28) (fig. S1, E to G) and OP9-DLL1 coculture (29) (fig. S1, H to J) in vitro systems. The presence of a *Bcl2* transgene in each system prevented the diminished survival that otherwise would have resulted from defective IL-7-STAT5 mediated induction of *Bcl2* in these DN cells. In the ATO system, deletion of either *Stat5a* or *Stat5b* partially lowered pSTAT5 in DN2 cells, and DN2 cells generated from *Stat5a*/*Stat5b*-deleted precursors showed greatly diminished IL-7-induced pYSTAT5, as expected (fig. S1, F and G). To measure the impact of STAT5 loss on CD25 expression, we generated mutant DN2 cells using the OP9-DLL1 co-culture T cell differentiation system as described (30, 31) (fig. S1H) and found that *Stat5a*/*Stat5b*-deletion reduced CD25 expression intensity across the stages (fig. S1I). Importantly, this effect on CD25 expression did not reflect a developmental block, given that *Stat5a/Stat5b*-deleted cells still underwent normally timed commitment to the T cell lineage, as shown by upregulation of a *Bcl11b-mCherry* reporter allele. By day 7, the control cells had progressed to the DN2 and early DN3 stages, with strong surface expression of CD25; however, when both *Stat5a* and *Stat5b* were deleted, both surface CD25 (fig. S1, I and J) and *Il2ra* RNA (fig. S1, K and L) expression were reduced in both pre-commitment ($BCL11b^{-}$) and post-commitment ($BCL11b^{+}$) DN2 stages. A global transcriptomic analysis showed that *Stat5a/Stat5b*-deficient DN2/3 cells had lower expression of growth and viability control genes (e.g., *Bcl2, Bcl2l1, Socs2, Cdkn1a, Eno1, Xbp1,* and *Bhlhe40*), as well as of *Il2ra* (Table S3), but the cells were not altered in their developmental progression (Table S3) as defined by a curated panel of markers, including *Tcf7, Bcl11b, Lck, Thy1, Cd3* clusters, *Ets1*, *Tcf12,* and *Rag* genes (32). This effect of STAT5 was in addition to the known requirement for Notch signaling to induce and sustain CD25 expression in DN thymocytes (fig. S1M; this panel is from (30) and shows lower CD25 when both *Notch1* and *Notch2* are disrupted). Thus, STAT5 activation cooperated with Notch signaling to induce and maintain normal *Il2ra*/CD25 expression in DN2-DN3 pro-T cells.

In vitro generated DN2 ($CD25^{+}cKit^{+}$) thymocytes responded to IL-7 with a STAT5 binding pattern similar to that observed in IL-2-stimulated $CD8^{+}$ T cells (Fig. 1A), but interestingly, steady-state thymic DN3 cells isolated *ex vivo* had their greatest STAT5 binding at the

upstream region of the super-enhancer, primarily at the UP3 element (Fig. 1A), a pattern distinct from that observed in IL-2-induced $CD8^+$ T cells or iTregs. Other factors including Notch/RBPJ (30, 33–35), RUNX1 (31, 36), BCL11b (37), and TCF-1 (38) are known to contribute to lineage progression to the DN2b-DN3 stages, and these factors bound in proximity to the STAT5 binding sites in DN2b-DN3 cells (fig. S2A), suggesting that they might cooperate to control the developmental regulation of *Il2ra* expression in DN cells. Additional transcription factors bound to these sites in mature T cells as well (discussed below; fig. S2B).

We next analyzed chromatin accessibility at the *Il2ra* locus throughout lymphoid development using ATAC-Seq (Assay for Transposase-Accessible Chromatin with high-throughput sequencing) datasets from the ImmGen database (39). Interestingly, an open chromatin region at upstream element UP3 (Fig. 1B; left red box) was detected in DN1 thymocytes, modestly increased in DN2a, DN2b, and DN3 thymocytes, but then was essentially absent in DN4 thymocytes; thus, the loss of chromatin accessibility at UP3 approximately correlated with the loss of CD25 expression. Accessibility at the intronic IN1m STAT5 binding site was relatively low in thymocyte populations, was greater in naïve CD4 and CD8 cells, Treg cells, NK cells, and ILC2s, but then was weak in splenic conventional DC and plasmacytoid DC (pDC) populations (Fig. 1B, right red box), suggesting differential use of upstream and intronic elements in different cellular populations.

Upstream super-enhancer elements are required for CD25 expression in DN thymocytes

To investigate the roles of the upstream and intronic enhancer elements in lymphoid development and function, we next deleted a range of individual elements or combinations of elements within the *Il2ra* super-enhancer (Fig. 2A) *in vivo* using CRISPR-Cas9 methodology. There was no significant effect on either thymic (fig. S3A) or splenic (fig. S3B) cellularity when individual upstream elements or even the entire UP1–6 upstream region (ΔUP1–6) or intron region (ΔIntron) or both together (ΔUP1–6/ΔIntron) were deleted, nor did they affect the percentage of DN thymocytes (fig. S3C). However, mice lacking the UP1–6 region had a profound decrease in the percentage of $CD25^+CD44^+$ DN2-phenotype and $CD25^+CD44^-$ DN3-phenotype thymocytes, whereas loss of the intron region had little effect (Fig. 2B). RNA-Seq analysis of DN thymocytes from WT, ΔUP1–6, or ΔUP1–6/ΔIntron mutant mice showed that *Il2ra* mRNA was essentially absent in the mutant mouse samples, but *Bcl11b, Tcf7,* and *Il7ra* mRNAs, which are normally expressed in DN2/DN3 cells (40), were still expressed (fig. S3D). This indicates that the DN2-DN3 stage pro-T cells were indeed still present but lacked CD25 expression due to deletion of essential *Il2ra* regulatory elements. Separate deletions of UP1, UP2, UP3, and UP5–6 did not affect CD25 expression in DN thymocytes (Fig. 2, C and D). Interestingly, however, deletion of the ΔUP2–3 region, which fully spans UP2 to UP3 and includes an RBPJ binding motif downstream of UP3 (TGACTAATG; chr2:11,623,400–11,623,408) that is occupied by RBPJ in DN2b/DN3 cells (30)(see fig. S2A), essentially eliminated CD25 expression on DN cells. We therefore generated mice lacking UP3 extending through the RBPJ site (ΔUP3-RBPJ) and found that this deletion also abrogated CD25 expression on DN thymocytes, phenocopying the ΔUP1–6 mice (Fig. 2, C and D). Thus, the UP3-RBPJ region

was indispensable for CD25 expression in DN thymocytes. To further analyze the role of the upstream elements, we cloned individual upstream enhancer elements in a reporter construct and analyzed reporter activity in a DN3-like cell line (SCID.Adh.2C2) (41, 42). In these cells, which spontaneously undergo Notch signaling, the UP3-RBPJ region was sufficient to drive reporter activity, and reporter activity was not augmented by stimulating the cells with IL-2, IL-7, or the combination of IL-2 with PMA + ionomycin (PI), which can mimic TCR stimulation (Fig. 2E). Strikingly, activity for all treatment conditions was significantly reduced when the STAT5 binding site (GAS motif), the RBPJ binding site, or both sites were mutated (Fig. 2F), or when a Notch inhibitor (γ-secretase inhibitor, GSI) was used (Fig. 2G). Even though *in vivo* deletion of the UP5-UP6 region had little if any effect, the UP5 element also exhibited modest reporter activity in these cells, with enhanced activity induced by IL-2, IL-7, PI, and PI/IL-2 (Fig. 2E), but inhibiting Notch had little effect on UP5 activity, indicating the specificity of the Notch inhibitor for effects via the UP3-RBPJ region (Fig. 2G). These results indicate a key role for the UP3-RBPJ element in regulating CD25 expression in DN2 and DN3 cells, with its activity requiring both STAT5 and Notch. In addition to the co-localization of RBPJ with STAT5 at the UP3 site, RUNX1, TCF1, and BCL11b, which are all involved in progression through DN thymocyte development, also bound at the UP3 region (fig. S2A), suggesting that multiple signals may be involved in the regulation of CD25 expression in DN2/DN3 thymocytes.

Differential control of CD25 expression on thymic and peripheral Treg cells

Because CD25 is also constitutively expressed on Treg cells, we next investigated whether *Il2ra* gene regulation in these cells was similar to what we observed in DN thymocytes. Thymic and splenic Treg cell numbers were not affected by any of the deletions (fig. S3, E and F), but deleting UP1–6 or both UP1–6 and intronic regions markedly reduced CD25 expression on both thymic and splenic Tregs (Fig. 3, A and B). Strikingly, whereas the ΔUP2–3 or ΔUP3-RBPJ deletions essentially abrogated CD25 expression on DN2/DN3 thymocytes (Fig. 2C), these deletions did not significantly affect CD25 expression on thymic Tregs (Fig. 3A) and only modestly lowered CD25 expression on splenic Tregs (Fig. 3B), indicating distinctive regulation of the *Il2ra* gene in DN thymocytes and Tregs. Interestingly, unlike splenic Tregs, ΔIntron thymic FoxP3$^+$ Tregs exhibited a bimodal pattern with a strong CD25-negative population (Fig. 3C, left and middle panels, and Fig. 3D), reminiscent of FoxP3$^+$CD25$^-$ thymic Treg precursor cells that normally activate CD25 expression in response to IL-2, IL-7, or IL-15 (43, 44). The biomodal pattern seen in ΔIntron Tregs in Fig. 3C suggests that cytokine-mediated induction of CD25 in precursor Tregs may be particularly dependent on the intronic region, with its deletion resulting in a higher percentage of CD25$^-$FoxP3$^+$ cells (Fig. 3, C and D). Consistent with this, when the total thymic CD4$^+$ cells were examined for Treg precursor populations, it was apparent that deletion of the intron led to a decreased percentage of CD25$^+$FoxP3$^-$ cells (fig. S3, G and H) but increased percentage of CD25$^-$FoxP3$^+$ cells (fig. S3, G and I). This CD25$^-$FoxP3$^+$ precursor population was increased in ΔIntron and ΔUP1–6/ΔIntron Tregs (Fig. 3D). Notably, neither the ΔIN1ab nor the ΔIN1m deletion had this effect, indicating that deletion of the entire ΔIntron region was required for the biphasic effect and increase in the CD25$^-$FoxP3$^+$ population (Fig. 3E). Although both upstream and intronic deletions affect the percentages of these two Treg precursor populations, neither deletion prevented

their differentiation to mature $CD25^{+}FoxP3^{+}$ Tregs (fig. S3, E and F); however, the level of CD25 expression (MFI) on the Tregs that emerged was significantly affected by the upstream deletion (Fig. 3, A and B). In another study, mice on a different background lacking an intronic enhancer (known as EDEL or CaRE4) also had decreased $CD25^{+}FoxP3^{-}$ precursor cells (45). Interestingly, although the ΔIntron and ΔUP1–6/ΔIntron exhibited biphasic CD25 peaks for thymic Tregs (Fig. 3C, left lower two panels), the higher CD25 component had an increased MFI in ΔIntron Tregs but not in ΔUP1–6/ΔIntron Tregs (Fig. 3C, middle panel). The bimodal pattern observed in ΔIntron Tregs was not as readily observed in splenic Tregs (Fig. 3C, right panel), indicating differences in CD25 regulation in thymic and splenic Tregs and suggesting that $CD25^{-}FoxP3^{+}$ Tregs in the thymus either do not exit to the periphery or are eliminated. Taken together, these results suggest that the *Il2ra* intronic sites are important for cytokine-mediated activation of *Il2ra* in Treg precursors while the UP1–6 region is important for controlling the magnitude of *Il2ra* expression in Tregs.

Interestingly, ΔIntron mice expressed lower levels of FoxP3 in thymic Tregs (fig. S3J), while ΔUP1–6 mice expressed lower levels of FoxP3 mainly in splenic Tregs (fig. S3K). This suggests that STAT5-activating cytokines such as IL-2, working through the high-affinity IL2Rαβγ complex, can regulate expression of FoxP3 in Tregs. This is consistent with evidence that a FoxP3 enhancer element containing STAT5 binding sites can mediate IL-2-regulated Treg function (46). In addition to the regulation of FoxP3 transcription by IL-2-induced STAT5 activation, FoxP3 binding sites were found at or near the STAT5 sites at the *Il2ra* intronic region (fig. S2B), suggesting a positive feedback regulation whereby IL-2 via STAT5 regulates expression of FoxP3, which in turn regulates *Il2ra* expression and thus responsiveness to IL-2 in the Treg lineage. Splenic Tregs with the ΔUP1–6 deletion had lower CD25 than WT Tregs or those with the ΔIntron deletion (Fig. 3C) and less potently suppressed $CD4^{+}$ T cell proliferation in vitro, as compared to WT or ΔIntron Tregs (Fig. 3, F and G), importantly correlating reduced CD25 levels and reduced levels of FoxP3 with impaired function in the Treg lineage. Tregs from ΔUP1–6 mice had similar viability to WT and ΔIntron Tregs at the end of the suppression assay (Fig. 3H), excluding death as the reason for reduced suppression. Taken together, these results indicate that peripheral Tregs depend on elements within the UP1–6 region for constitutive *Il2ra* expression, but the critical elements within the UP1–6 region are at least partially distinct from those required for *Il2ra*/CD25 expression by DN thymocytes. However, the likelihood of *Il2ra* activation in this lineage in the thymus and the extent of STAT5-dependent Foxp3 upregulation depends on the integrity of the super-enhancer intron region.

Inducible CD25 expression on $CD8^{+}$ and $CD4^{+}$ T cells is controlled by super-enhancer intronic elements

We next assessed the effects of upstream and intron deletions in the super-enhancer on inducible CD25 expression in peripheral $CD8^{+}$ T cells. In freshly isolated WT $CD8^{+}$ T cells, IL-2 induced *Il2ra* mRNA expression, with greater induction at 1000 U/ml than 100 U/ml IL-2 in these $CD8^{+}$ T cells (fig. S4A). Cells from ΔUP1–6 mice exhibited similar induction with 100 U/ml IL-2, but for unclear reasons, unlike WT cells, the response was reproducibly not further increased with 1000 U/ml IL-2. Strikingly, the intron deletion

abolished IL-2-induced *Il2ra* mRNA expression (fig. S4A). We next investigated the roles of the individual upstream or intronic elements in cell surface CD25 expression in response to IL-2 in $CD8^+$ T cells, either in the absence or presence of anti-CD3 + anti-CD28 stimulation. IL-2-induced CD25 expression at day 2 of culture generally paralleled *Il2ra* mRNA expression, with much lower CD25 expression on the ΔIntron or ΔUP1–6/ΔIntron cells (Fig. 4A, left 3 sets of flow profiles, and Fig. 4B). When cells were stimulated with anti-CD3 + anti-CD28 and then IL-2, CD25 expression was much higher (Fig. 4A, right 3 sets of flow profiles, and Fig. 4B), but deleting the intron essentially eliminated CD25 expression (Fig. 4B). The upstream region also contributed to CD25 inducibility, particularly at 4 days (Fig. 4C and fig. S4B). None of the individual upstream deletions decreased CD25 expression as much as the larger ΔUP1–6 deletion (Fig. 4, A and B), suggesting that elements within this region cooperatively modulate CD25 expression in $CD8^+$ T cells, but even ΔUP1–6 did not affect expression nearly as much as deleting the intronic region. Thus, the intron region contains the major elements responsive to TCR and IL-2 signals in $CD8^+$ T cells. This region includes a TCR-responsive intronic element approximately 200 bp from the 3' end of IN1a (22) as well as TCR-responsive NFATc1 sites that colocalize with each of the intronic STAT5 sites (fig. S2B) all of which are deleted in the ΔIntron deletion. Deletion of both IN1a and IN1b, or of IN1m (fig. S4C), or of the element described by Simeonov (22) each had more modest defects on CD25 expression than deletion of the entire intron region, suggesting that the intronic elements functionally cooperate to mediate high level IL-2-induced *Il2ra* expression in $CD8^+$ T cells.

Because naïve $CD4^+$ T cells do not express IL-2Rα and have lower expression of IL-2Rβ than naïve $CD8^+$ cells, they cannot substantially respond to IL-2 prior to activation (47). We therefore analyzed the effects of *Il2ra* upstream and intron deletions on the $CD4^+$ T cell response to anti-CD3 + anti-CD28, which augments expression of IL-2Rα and IL-2Rβ. In contrast to the IL-2-induced CD25 expression in $CD8^+$ T cells co-stimulated with anti-CD3 + anti-CD28 (Fig. 4A–4C), in WT $CD4^+$ T cells, CD25 was strongly expressed after TCR stimulation, with no further increase induced by IL-2 (Fig. 4, D and E). This was presumably at least in part due to endogenous IL-2 production induced by TCR signaling in $CD4^+$ T cells. Flow cytometric analysis revealed an essential role for the intron and a partial role for UP1–6 for the induction of CD25 in $CD4^+$ T cells (Fig. 4, D and E), similar to their roles in $CD8^+$ T cells. As compared to WT, individual deletion of UP3-RBPJ and to a lesser extent UP2 and UP5–6 each had partial effects on CD25 expression in $CD4^+$ T cells (Fig. 4E). However, deleting IN1a and IN1b together or IN1m had essentially no effect, in contrast to the effect of deleting the combined region (ΔIntron) (fig. S4D), suggesting some redundancy among the elements in this critical region in $CD4^+$ cells.

As noted above, CD25 expression on splenic Tregs was primarily dependent on the UP1–6 region, with no evidence for a contribution of the intron region (Fig. 3B). To examine Tregs in more detail, we also generated induced Tregs (iTregs) by stimulating naïve $CD4^+$ T cells isolated from spleens with TGFβ, IL-2, anti-IFNγ, and anti-IL-4 (see Methods). Like splenic Tregs, for iTregs, ΔIntron alone had no effect and ΔUP1–6 significantly reduced CD25 expression, but the loss of both regions further reduced CD25 expression (Fig. 4F). Thus, although generated from peripheral T cells, conversion to iTregs induced a major switch in the elements used for *Il2ra* regulation as compared to those used by peripheral

effector CD4$^+$ T cells that were TCR-stimulated in the absence of TGFβ. None of the individual upstream elements was solely responsible for the lower CD25 expression in iTregs observed with ΔUP1–6 (Fig. 4F).

Because iTregs are induced in the presence of TGFβ, we examined WT CD4$^+$ T cells activated with anti-CD3 + anti-CD28 in the presence of IL-2, TGFβ, or both TGFβ and IL-2. Compared to anti-CD3 + anti-CD28, the addition of IL-2 had little effect, and although the addition of TGFβ repressed CD25, combining IL-2 with TGFβ reversed this repression, restoring CD25 expression to the level observed with anti-CD3 + anti-CD28 (fig. S4, E and F). Similar qualitative effects were observed with cells from ΔUP1–6 mice, but interestingly, CD4$^+$ (fig. S4, E and F) and CD8$^+$ T cells (fig. S4, G and H) from ΔIntron mice had minimal responses to IL-2, whereas the combination of TGFβ with IL-2 had a strong cooperative effect on CD25 expression on ΔIntron cells, partially compensating for the loss of the intron (fig. S4, E–H). Because of the effect of TGFβ, we reasoned that SMAD4 might bind to the *Il2ra* super-enhancer region. We previously identified a TGFβ responsive element in an upstream proximal promoter region that we denoted positive regulatory region 5, PRR5 (48), and when we examined published ChIP-Seq data for SMAD4, we found SMAD4 binding sites throughout the *Il2ra* locus in Th17 cells (49) (fig. S2B), co-localizing with STAT5 binding sites in the intron and others, including at PRR5. These latter SMAD4 sites potentially operate independently of the intronic region and might help to explain the difference in intron-dependence of CD25 expression in CD4$^+$ T cells versus iTregs. In addition to the colocalization of transcription factors involved in transmitting signals from cytokines or the T cell receptor, TCF1, which is involved in T cell lineage maturation, had partially overlapping and partially distinctive binding profiles at the super-enhancer during thymic development versus naïve CD8$^+$ T cells (fig. S2B). These data collectively indicate that multiple signals converge at distinct regions of this gene, potentially serving to differentially modulate CD25 expression in different lineages.

Il2ra super-enhancer intronic elements control cytokine-induced CD25 expression on NK cells

NK cells potently respond to IL-15 as well as IL-2, with IL-15 and STAT5 being critical for the development and proliferation of these cells (25, 50, 51). Although CD25 expression is normally low in NK cells, IL-12 can augment CD25 expression in NK cells both in vivo and in vitro (52). We therefore examined CD25 induction in splenic NK cells cultured with IL-15 without or with IL-12 and found cooperative induction (see fig. S5A for day 4 and fig. S5B for days 2 and 4). As anticipated, IL-15-stimulated NK cells expressed *Il2ra* mRNA, with much higher levels induced by IL-15 + IL-12 (fig. S5C), although even this level of mRNA expression corresponded to levels of CD25 protein expression (fig. S5B) that was still significantly lower than the level induced by IL-2 on WT CD8$^+$ T cells based on a comparison of MFIs (Fig. 4C). As compared to WT NK cells, NK cells from the ΔIntron and ΔIntron/ΔUP1–6 mutant mice had markedly decreased CD25 expression in response to IL-15 + IL-12, down to the level of cells stimulated only with IL-15, whereas ΔUP1–6 NK cells were closer in their response to WT cells at both the protein (fig. S5B) and mRNA (fig. S5C) levels. Thus, the intronic region but not the UP1–6 region appears to mediate cytokine-stimulated *Il2ra* expression in NK cells.

Mice lacking the *Il2ra* upstream enhancer elements develop alopecia

Because mice with complete deletion of *Il2ra* expression develop spontaneous multi-organ autoimmune disease (53) and deletion mutants of the *Il2ra* super-enhancer elements have distinctive effects on CD25 expression levels at different stages of development including on Tregs, we surveyed our panel of mouse *Il2ra* deletion mutants for phenotypic changes indicative of autoimmune responses. Strikingly, the ΔUP1–6 mice spontaneously developed well-demarcated areas of alopecia (Fig. 5A), and this was not observed in any of the other mutants. This phenotype was reminiscent of alopecia areata, a T cell mediated autoimmune disease characterized by patchy hair loss that is mediated by $CD8^+$ T cells, with a subset of patients associated with single nucleotide polymorphisms in *IL2RA* (54, 55). Tregs from the ΔUP1–6 mice had defective expression of CD25 and immunosuppressive activity (Fig. 3), which could contribute to development of an immune-mediated alopecia, with destruction of hair follicles. The alopecia in ΔUP1–6 mice developed in both males and females, typically at approximately 10 to 12 weeks of age, with a prevalence of approximately 30%. We next analyzed affected skin lymphoid populations in WT, ΔUP1–6, and ΔIntron mice by flow cytometric analysis of isolated skin cells and found significantly higher percentages of $CD45^+$ hemopoietic cells as well as $CD8^+$ T cells in alopecia skin (Fig. 5, B and C). Consistent with the reduced responsiveness of ΔIntron $CD8^+$ T cells, ΔIntron mice had a significantly reduced percentage of $CD8^+$ T cells in the skin (Fig. 5, B and C). In contrast, $FoxP3^+$ Tregs, which normally comprise approximately 50% of the $CD4^+$ T cells in normal skin (56), were reduced in the skin of ΔUP1–6 mice with alopecia skin but were increased in the ΔIntron skin, as compared to WT skin (Fig. 5, B and C). The overall percentage of $CD25^{high}CD4^+$ T cells was reduced in alopecia skin from ΔUP1–6 mice (Fig. 5C), consistent with the reduced CD25 expression on Tregs in these animals (Fig. 3). Immunohistochemistry revealed increased hair follicle accumulation of $CD4^+$ T cells in both ΔUP1–6 and ΔIntron mice, but prominent $CD8^+$ T cell infiltration was found only in the ΔUP1–6 mice (Fig. 5D), consistent with $CD8^+$ T cell-dependent alopecia and with defective function of Tregs in these animals. Interestingly, ΔUP1–6/ΔIntron mice lacking both the upstream and intronic enhancer regions did not develop alopecia. This was presumably because even though their Tregs had reduced immunosuppressive ability, their $CD8^+$ T cells were also defective in their proliferative responses due to the effect of the intronic deletion and hence could not cause hair follicle destruction. The alopecia that was evident in the ΔUP1–6 mice was not the result of hyperactivated $CD8^+$ T cells, as levels of CD62L and CD44 were the same as in WT $CD8^+$ T cells in both the spleen and mesenteric lymph node (Fig. S6, A and B). Additionally, a range of other organs were characterized histologically in these mice and there was no evidence of pathological changes (Fig. S6C).

To further characterize the immune cell infiltrates in the skin, we conducted single-cell RNA-sequencing (scRNAseq) on sorted skin-infiltrating $CD45^+$ cells from WT and ΔUP1–6 mice with or without alopecia. Unsupervised clustering on combined datasets from each strain using Seurat categorized the cells into 13 clusters, which were annotated based on the gene expression patterns (Fig. 5E; fig. S7, A and B; Table S4). Clusters 1 to 4 and 6 represented lymphoid lineages, where Cluster 1 contained several cytotoxic likely including NK cells, type 1 innate lymphoid cells (ILC1s), and a subset of CD8 T cells. Cluster 2 included CD4 and CD8 T cells, as well as group 2 and 3 ILCs. Cluster 3 was annotated

as gamma delta T17 cells, Cluster 4 was identified as Tregs, and cluster 6 as dendritic epidermal T cells. There was little gross change in the representation of these clusters among WT skin, skin from ΔUP1–6 mice with alopecia, and skin from ΔUP1–6 mice without alopecia, and all major cell types were captured from each strain (fig. S7C).

Comparing Tregs from WT mice and ΔUP1–6 mice with alopecia revealed that there was a short list of genes that were differentially expressed (Table S4). Nevertheless, ΔUP1–6 Tregs, with or without alopecia, as compared to WT Tregs, were characterized by the downregulation of *Il2ra* (Fig. 5F), consistent with our findings in the thymus and spleen (Fig. 3, A and B, Table S4). *Ly6e* was among the most potently downregulated genes, and upregulated genes included *Ifnar2* and *Il7r*, implying enhanced responsiveness to type 1 IFNs and IL-7.

We then compared the Tconv/ILC clusters from ΔUP1–6 with or without alopecia to the corresponding WT cluster and derived differentially expressed genes (DEGs). This analysis revealed 64 upregulated and 209 downregulated genes in ΔUP1–6 alopecia mice, but there were fewer DEGs (19 upregulated and 32 downregulated genes) in ΔUP1–6 without alopecia (Fig. 5G). Analysis of the DEGs revealed that 54 upregulated and 181 downregulated DEGs were unique to the Tconv/ILC cluster from ΔUP1–6 alopecia mice (Fig. 5G). Metascape pathway analysis of the list of unique DEGs revealed upregulation of pathways for leukocyte differentiation, myeloid leukocyte differentiation, and IL-2 signaling pathways, and downregulation of pathways for regulation of immune effector process, regulation of lymphocyte activation, and adaptive immune response (Fig. 5H). Genes that were uniquely upregulated by ΔUP1–6 alopecia mice included *Il7r*, *Ccr6* and *Gata3*, and those uniquely downregulated included *Bcl2a1d*, *Abcb1b*, and *Dusp5* (Fig. 5I, Table S4).

Intronic elements control the chromatin structure of the *Il2ra* super-enhancer

We next wished to further evaluate the roles of these regulatory elements in the overall chromatin structure of the locus. The ATAC-Seq data showed that the intronic IN1m region had an open chromatin structure throughout lymphoid development, and UP3-RBPJ was accessible in DN2 and DN3 but not in DN4 thymocytes (Fig. 1B), correlating with CD25 expression. Histone-3-lysine27-acetylation (H3K27Ac), which is a mark of active enhancers (57), was evident in DN3 thymocytes from *Rag2* KO mice and in DN thymocytes from WT mice. In these cells, within the upstream region, it was enriched at UP3-RBPJ (green tracks, top of Fig. 6A) and deleting the intronic region (ΔIntron) in DN thymocytes did not substantially affect H3K27Ac in the upstream region (Fig. 6A), consistent with the upstream rather than intronic region controlling constitutive CD25 expression on DN2-DN3 thymocytes (Fig. 2B). In WT $CD8^+$ T cells, H3K27Ac was more broadly distributed throughout the *Il2ra* super-enhancer region, and deleting the intron region reduced H3K27Ac levels throughout the *Il2ra* locus, including at the upstream region, whereas deleting UP1–6 resulted in a loss of H3K27Ac signal mapping to the upstream region as expected but had little if any effect in the intronic region (Fig. 6A). As expected, the changes in chromatin structure were specific to the *Il2ra* locus; for example, the various *Il2ra* deletions did not affect the H3K27Ac binding profile at the locus for another IL-2-induced gene, *Cish* (fig. S8A).

We also evaluated H3K27Ac marks at the *Il2ra* locus in WT, ΔIntron, and ΔUP1–6 NK cells stimulated with IL-15 or IL-15 + IL-12 and found that they were primarily in the promoter and intronic regions and not evident in the upstream region (bottom six tracks, Fig. 6A). H3K27Ac binding intensity at the *Il2ra* locus was enhanced in NK cells stimulated with IL-15 + IL-12 as compared to stimulation with IL-15 alone (Fig. 6A), consistent with augmented protein and mRNA expression (fig. S5, A–C). This enhancement was also associated with greater numbers of total STAT5 binding sites identified by ChIP-Seq analysis in NK cells stimulated with IL-15 + IL-12 versus IL-15 alone (fig. S8, B and C). Interestingly, deleting either the UP1–6 region or the intron led to the loss of H3K27Ac marks throughout the *Il2ra* gene in NK cells (Fig. 6A), indicating the importance of both regions for controlling *Il2ra* expression in these cells. Consistent with the observation that *Il2ra* gene expression is significantly lower in NK cells than in $CD8^+$ T cells or $CD4^+$ T cells, an analysis of STAT5-bound super-enhancers in $CD8^+$ and NK cells showed that the super-enhancer score of the gene was ranked first in $CD8^+$ T cells but was only 151^{st} in NK cells (fig. S8, D and E).

These observations demonstrate that the enhancer activity and chromatin structure at the *Il2ra* gene are dynamic, with substantial variation during lymphoid development and in different cell types, suggesting a potential hierarchical chromatin organization within this super-enhancer. The intronic element influences the chromatin interactions of the locus and expression in $CD8^+$ T cells and NK cells, whereas the upstream super-enhancer elements seemed to exhibit broad effects but were most dramatically required for *Il2ra* expression in thymic DN2 and DN3 cells and in Tregs, with lesser effects in $CD8^+$ T cells, consistent with normal *Il2ra* expression in DN thymocytes from ΔIntron mice. Note that for $CD8^+$ T cells, TCR activation resulted in strong H3K27Ac, with little subsequent effect of IL-2 (Fig. 6A). This is consistent with our previous observations that IL-2 augments STAT5 binding but has no evident further effect on H3K27Ac (21).

Recruitment of MED1 by the *Il2ra* super-enhancer

Strong binding of MED1, a core component of the Mediator co-activator that is required for the activation of RNA polymerase II, is characteristic of super-enhancers (2). We therefore analyzed the profile of MED1 binding to the *Il2ra* super-enhancer in various cell types. In DN3 thymocytes and in a DN3 cell line, which constitutively express CD25 and have strong STAT5 binding at UP3 with closely juxtaposed RBPJ binding (Fig. 1), there was significant MED1 binding to the UP3 element (Fig. 6B). In WT $CD8^+$ T cells stimulated with IL-2, MED1 partially co-localized with STAT5B binding in both the upstream and intronic regions (Fig. 6B). Genome-wide analysis of STAT5B and MED1 binding in $CD8^+$ T cells revealed that 44% of genes bound by STAT5 also had co-binding of MED1 (fig. S9A), suggesting possible cooperation between these factors. We examined published RNA-Seq data from preactivated $CD8^+$ T cells that were stimulated with IL-2 for 48 hours (58) and found that 25% of the 100 most-inducible genes were co-bound by STAT5 and MED1, including *Cish* and *Il2ra* (fig. S9B). We next examined the binding of the cohesin complex component RAD21, given the ability of RAD21 and MED1 to form a complex, connecting gene expression and chromatin architecture (59). Indeed, consistent with the binding pattern observed for MED1 (Fig. 6B), there was significant binding of RAD21 at the UP3 and

intronic regions in wild-type $CD8^+$ T cells upon IL-2 stimulation. Interestingly, binding at both sites was attenuated with deletion of either the intron or UP1–6 region (fig. S9C). Furthermore, ΔIntron $CD8^+$ T cells had essentially no MED1 binding throughout the *Il2ra* locus (Fig. 6B), consistent with attenuated H3K27Ac marks (Fig. 6A) and suggesting that deleting the intron disrupted the super-enhancer structure in these cells. Thus, efficient binding of mediator and cohesin complex components to the super-enhancer involves interactions with both the intron and UP1–6 regions.

There was only weak MED1 binding in NK cells cultured with or without IL-15 (Fig. 6B), consistent with the lower CD25 protein expression on IL-15-stimulated NK cells (fig. S5B) than on IL-2-stimulated $CD8^+$ T cells (Fig. 4C). Treg cells constitutively express CD25 and had a MED1 binding profile relatively similar to that observed in IL-2-induced $CD8^+$ T cells (Fig. 6B). These results collectively underscore the differential use of elements within the super-enhancer during lymphoid development and/or cytokine stimulation.

To further investigate the role of the higher order chromatin structure at the *Il2ra* locus, we performed H3K27Ac HiChIP experiments using $CD8^+$ T cells stimulated with anti-CD3 + anti-CD28. These experiments revealed significant H3K27Ac-mediated chromatin interactions among the *Il2ra* promoter, the upstream and the intronic cis-regulatory elements, with increased looping in the presence of IL-2 (Fig. 7, A and B) in WT cells. Interestingly, there was also looping to the adjacent *Il15ra* gene, although RNA-Seq or RT-PCR showed no significant decline *in Il15ra* expression in $CD8^+$ T cells, $CD4^+$ T cells or NK cells from WT, ΔIntron, and ΔUP1–6 mice. Instead, *Il15ra* expression was either similar ($CD4^+$ T or NK cells) or perhaps slightly higher in the mutants in $CD8^+$ T cells (Fig. S9D), an observation worthy of future investigation. The ΔIntron cells not only lacked all loops from within the intron region (as expected) but had greatly reduced looping from the upstream region to the *Il2ra* promoter (Fig. 7A), which in part may reflect the lower H3K27Ac (Fig. 6A). Conversely, ΔUP1–6 eliminated all loops from within the upstream region, but it had relatively little effect on looping from the intron to the promoter (Fig. 7A). Other IL-2-induced gene loci showed no difference in looping (e.g., the *Bcl2* locus; Fig. 7, C and D), confirming that the changes in chromatin interactions were specific to the *Il2ra* locus. These data underscore important contributions of both the intronic and upstream super-enhancer regions to the regulation of the *Il2ra* gene in mature T cells, with our data indicating key roles for the intronic region for effector cells and the upstream region for Treg cells, consistent with alopecia in mice lacking the upstream region.

Discussion

We have extensively dissected the *Il2ra* super-enhancer *in vivo* and identified regulatory elements that differentially control gene expression in distinct cellular lineages and at different stages of lymphoid development, as well as in response to different cytokines. Strikingly, the upstream region controls constitutive CD25 expression during early thymic development and Treg cells, but it contributes to expression in all lymphoid cell types studied. In this region, we identified a Notch-responsive element that controls constitutive DN2/DN3 thymocyte CD25 expression and cooperates with STAT5, thus linking Notch signaling to a STAT5-regulated transcriptional event. Moreover, Notch

signaling is important for T-cell commitment in the thymic microenvironment, and the acquisition of CD25 expression is thus linked to the Notch signal (60, 61). Strikingly, alopecia occurred in mice lacking the upstream but not the intronic super-enhancer region. This was associated with downregulation of *Il2ra* in Tregs, as well as a transcriptomic shift in the Tconv/ILC cluster that was characterized by upregulated pro-inflammatory and downregulated immunoregulatory pathways. However, scRNA-seq analysis of human alopecia areata and an alopecia areata mouse model (C3H/HeJ mice) that is mediated by $CD8^+$ T cells exhibit more exuberant inflammatory and cytotoxic features than were evident in our ΔUP1–6 alopecia mice (62). It is possible that there are different grades of inflammatory responses in subsets of human alopecia areata that are influenced by genetic predispositions, and conceivably our mouse model may correspond to the subset of human alopecia areata patients with single-nucleotide polymorphisms in the *IL2RA* locus. The incomplete penetrance of alopecia in ΔUP1–6 mice remains unexplained but suggests that an additional hit, possibly environmental, is required for the development of the phenotype, an area for future study.

Unlike the upstream super-enhancer region, the intronic region was most critical for cytokine-inducible *Il2ra* expression in $CD8^+$ T cells (IL-2), in NK cells (IL-15 or IL-15 +IL-12), and in $CD4^+$ T cells preactivated with anti-CD3 + antiCD28 (IL-2). Individual deletion of the intronic STAT5 binding sites had only minor effects on *Il2ra* mRNA expression, indicating that the elements cooperate for full expression. Moreover, deletion of the intron disrupted chromatin structure throughout the *Il2ra* locus, with reduced MED1 and H3K27Ac binding. In contrast, deleting the intron did not affect CD25 expression on DN2/DN3 thymocytes, indicating that the structure of the super-enhancer may evolve as thymocytes develop to mature T cells. In analyzing progression through thymic development, we found that STAT5 is required for normal CD25 expression in the earliest DN stages. Moreover, STAT5 co-localizes with other transcription factors (NOTCH, RUNX, BCl11b, TCF1) that facilitate development. It is likely that some of these individually or in combination associate with other nuclear proteins that orchestrate chromatin accessibility and that such pioneer factors allow cytokine-dependent recruitment of STAT5 to these sites. This situation may be analogous to that in developing Tregs where FOXP3 binds to previously established enhancers to orchestrate a functional transcriptional program (63). Indeed, lower CD25 expression on Tregs correlates with lower suppression, and FOXP3 binds to both intronic and promoter-proximal *Il2ra* STAT5 site regions, suggesting that FOXP3 may contribute to *Il2ra* induction and thus to a positive feedback loop.

Context-dependent regulation of genes ranging from *even-skipped* in Drosophila to *Myc* in mammals is mediated by tissue-specific activities of distinct enhancers, sometimes widely separated in the genome (64–68). However, super-enhancers are usually identified by the simultaneous activity of distinct cis-regulatory elements within the same cellular context. Here, we show that the *Il2ra* super-enhancer comprises both modes of regulation. Some super-enhancers have individual enhancer elements that function in an additive fashion (3, 69), while others possess hierarchical structures in which individual elements are dominant (70). Our data indicate that the *Il2ra* super-enhancer intronic region functions as a hub in mature T cells, with increased occupancy of STAT5 binding sites and enhanced histone modifications associated with active chromatin, consistent with effects on the entire locus

when the intron is deleted. MED1 co-localized with STAT5 protein at three intronic sites, and this association was induced by IL-2. Moreover, MED1 binding correlated with *Il2ra* transcriptional activity, with lower binding in NK cells than mature $CD8^+$ T cells. Cohesin co-localized at STAT5 binding sites in the intron and at UP3, perhaps indicating co-occupancy of these factors at super-enhancer condensates. STAT proteins have been shown to be incorporated into nuclear condensates following cytokine stimulation (71), and cohesin and MED1 have been shown to function as coactivators in a complex of proteins that bind with lineage-specific or inducible transcription factors at enhancers of active genes, leading to the distinctive architecture of chromatin proteins that define the super-enhancer structure (59, 71). In $CD8^+$ T cells, deletion of the intron diminished the binding of MED1 and cohesin throughout the super-enhancer , and cohesin was also reduced throughout the locus by the UP1–6 deletion, suggesting that these mutant forms of the locus may be displaced from the super-enhancer condensate.

Overall, our findings underscore that the *Il2ra* super-enhancer, which is the highest ranked STAT5-based super-enhancer in both IL-2-induced $CD4^+$ and $CD8^+$ T cells (21), critically regulates gene expression, with regions that influence expression in distinct populations, clarifying the basis for differential *Il2ra* regulation in distinct cell types. More broadly, they illustrate how distinct elements within a super-enhancer can control constitutive versus inducible gene expression in different cell types. Although the super-enhancer organization is similar in mouse and human, most elements are not rigorously conserved (21). There are multiple autoimmune-related SNPs at the *Il2ra* gene locus (72), but so far, only one human SNP associated with protection from type 1 diabetes has been studied; this SNP delayed TCR-induced CD25 expression in T cells but did not affect steady state CD25 levels on Tregs, and the mechanism for protection from type I diabetes remains unclear (22). In contrast to this SNP, deleting UP1–6 resulted in alopecia, with reduced CD25 on peripheral Tregs. Although FoxP3 levels in thymic Tregs were mildly affected in ΔIntron mice, FoxP3 levels in splenic Tregs were more affected in ΔUP1–6 mice, suggesting developmental differences in the IL-2 inducibility of the FoxP3 gene in these animals, with decreased function of peripheral Tregs in the ΔUP1–6 mice. The lack of alopecia in ΔIntron mice makes sense as Tregs were reasonably intact and $CD8^+$ T cells had diminished CD25. Alopecia was also not observed in ΔUP1–6/ΔIntron mice, suggesting that the defect in $CD8^+$ T cells prevented hair follicle destruction, despite the defective Tregs in these animals.

Interestingly, the *Il2ra* elements bound by STAT5 differ across cell types, with variations in occupancy of upstream versus downstream elements in $CD8^+$ T cells versus Treg cells or DCs. Accordingly, selective interference with binding at key positions can be predicted to differentially affect CD25 expression in a cell type-related fashion, with presumed parallels in the human and potentially in human disease. For example, intronic mutations/deletions can be predicted to affect CD25 expression on NK cells and potentially impact innate immunity, whereas upstream mutations/deletions might instead impact Treg function and thus autoimmunity, an area for future investigation. Thus, the differential roles of upstream elements (e.g., for Tregs) versus intronic elements (e.g., for effector $CD8^+$ T or NK cells) might allow differential effects on CD25 expression in distinct cell types, with potential therapeutic utility.

Materials and Methods

Study design

This study investigated the *Il2ra* super-enhancer and mechanisms by which cell-type specific or developmental specific expression of this gene is controlled. Transcriptional studies and chromatin structural analyses in specific CRISPR-deletion mutants of the gene were used to elucidate mechanisms for controlling expression in multiple cell lineages. Intronic super-enhancer elements were shown to control *Il2ra* expression in peripheral $CD4^+$ and $CD8^+$ T cells, whereas upstream enhancer elements were shown to control expression of *Il2ra* expression in DN thymocyes and Treg cells. The functional consequences of deletions within the upstream region included the development of autoimmune alopecia. Sizes of experimental groups and number of repetitions are indicated in figure legends.

Mice

CRISPR-Cas9 mutant mice were generated by the transgenic core of the National Heart, Lung, and Blood Institute (NHLBI), as described (21). All experiments at NHLBI were performed using protocols approved by the NHLBI Animal Care and Use Committee and followed NIH guidelines for use of animals in intramural research. The sequence coordinates for each deletion mutant mouse are in Table S5. For in vitro derived DN2-DN3 cells with acute *Stat5a; Stat5b* deletion, mice combining a *ROSA26-Cas9* knock-in and a *Bcl2* transgene were bred at the California Institute of Technology from B6.Cg-Tg(BCL2)25Wehi/J(Bcl2-tg) and B6.Gt(ROSA)26Sortm1.1(CAG-cas9*,-EGFP)Fezh/J (Cas9) mice, originally purchased from the Jackson Laboratory. When a Bcl11b reporter allele was required, mice were bred with B6. $Bcl11b^{mCh/mCh}$ (mCherry) reporter mice (31). All protocols followed NIH Guidelines and were approved by the California Institute of Technology Animal Care and Use Committee.

Cell isolation and culture

$CD4^+$, $CD8^+$ and Tregs were isolated using StemCell Technologies kits. NK cells were purified from spleens using a Miltenyi kit and expanded in IL-15 (10 ng/ml) for 10 days for use in ChIP-Seq experiments. For short-term analysis of NK cells, purified NK cells were incubated with IL-15 (10 ng/ml) without or with IL-12 (10 ng/ml) for 2–4 days. $CD8^+$ T cells were cultured in RPMI-1640 medium containing 10% FBS and stimulated with IL-2 (100 or 1000 U/ml) or anti-CD3/anti-CD28 for 2 days, rested 4 hours, and IL-2 was added for the indicated times. For iTreg cultures, naïve $CD4^+$ T cells were isolated from spleens and cultured with anti-CD3/anti-CD28, TGFβ (2 ng/ml), IL-2 (1000 U/ml), anti-IFNγ (10 μg/ml), and anti-IL-4 (10 μg/ml) for 4 days. DN thymocytes were enriched by depleting total thymus with anti-CD4 and anti-CD8 antibodies (Miltenyi). Enriched DN3 cells were isolated from *Rag2* KO mice. Splenic DCs were purified using a Miltenyi kit, rested for 1 h, and stimulated with GM-CSF (20 ng/ml) for 2 h. Bone marrow-derived mast cells were generated by culturing bone marrow from femurs for 4–6 weeks in medium containing 10 ng/ml stem cell factor and 10 ng/ml IL-3; cells were sensitized with 0.5 μg/ml IgE (557079, Sigma) overnight, and stimulated with 50 ng/ml DNP-HSA (human serum albumin)(A6661, Sigma).

Treg suppression assay

5×10^4 Cell Trace Violet-labeled $CD4^+$ T cells were cultured with irradiated APC (2000 rads) and soluble anti-CD3 (1 μg/ml) in the presence of purified splenic Tregs from WT or CRISPR-Cas9 deleted mice. $CD4^+$ T cells and splenic Tregs were purified using Stem Cell Technology kits. APC were prepared by depleting $CD4^+$ and $CD8^+$ T cells from spleen using Miltenyi Biotec magnetic beads. $CD4^+$ T cells were labeled with Cell Trace Violet (Life Technologies) according to the manufacturer's protocol. The CD4:Treg ratio of displayed flow cytometry profiles for CTV dilution was 2:1. APC were present in a 5-fold excess over $CD4^+$ T cell numbers.

Reporter assays

DN3 SCID.Adh.2C2 cells that constitutively undergo Notch signaling and express CD25 were used (42)(35). 5×10^6 cells were electroporated with 2 μg of reporter plasmid containing constructs cloned 5' of the minimal promoter of pNL3.1 and 0.2 μg pNL-TK in 20 μl buffer using Lonza P3 primary cell kit for 4D Nucleofector. Cells were immediately stimulated with cytokine for 24 hr and nanoluciferase activity measured relative to control activity using the NanoGlo Dual Luciferase kit (Promega).

Single cell RNA-sequencing analysis

Freshly prepared cell suspension from the whole skin of C57BL/6 or ΔUP1–6 mouse were FACS sorted for $CD45^+$ immune cells (FACSAria Fusion, BD Biosciences). Droplet-based scRNA-seq captures and library preparations were performed with 10X Chromium 3' V2 kit (10X Genomics) according to the manufacturer's protocol. Reads were aligned to mouse reference genome mm10 using a STAR aligner to produce the digital gene expression matrix (10x Genomics Cell Ranger). Seurat R package (72) was used for further analysis with default parameters unless otherwise indicated. Quality control metrics excluded cells with >10% mitochondrial gene load, <200 total genes, and >5000 total genes. Each sample was then Log normalized (NormalizeData function) and Scaled (ScaleData function, including a linear regression of 'mitochondrial gene percentage' to reduce sources of variation). The top 2000 highly variable genes were used for canonical correlation analysis (CCA) implemented in Seurat to align samples using 15 principal components. Cell clustering was performed by 'FindClusters' function and dimensionality reduction was performed with 'RunUMAP'. DEGs were obtained using function 'FindMarkers', calculated by using the non-parametric two-sided Wilcoxon rank sum test in Seurat, and filtered with adjusted p values <0.05. Log-normalized gene expression count was used for visualizations of projected gene expression on dimensionality reduction plot using 'FeaturePlot' function. Violin plots were generated by ggplot2 package using log-normalized gene expression value.

ChIP-Seq and RNA-Seq analysis

ChIP-Seq experiments were performed as described (21, 73) using anti-STAT5B (Invitrogen 13–5300), anti-H3K27Ac (Diagenode), anti-MED1 (Bethyl A300–793A), anti-RAD21 (Abcam 217678), and anti-H3K4me1 (Abcam 176877). Libraries were prepared using the KAPA HyperPrep kit (Roche) and indexed with Illumina primers. PCR products were bar-coded (indexed) and sequenced using a HiSeq 2500 or NovaSeq6000 (both Illumina).

Sequenced reads (50 bp, single end) were obtained with the Illumina CASAVA pipeline and mapped to the mouse genome mm10 (GRCm38, Dec. 2011) using Bowtie 2.2.6 (74) and Tophat 2.2.1 (75). Only uniquely mapped reads were retained. The mapped outputs were converted to browser-extensible data files, which were then converted to binary tiled data files (TDFs) using IGVTools 2.4.13 (76) for viewing on the IGV browser (http://www.broadinstitute.org/igv/home). TDFs represent the average alignment or feature density for a specified window size across the genome. For ChIP-Seq data, we mapped reads into non-overlapping 20 bp windows for various transcription factors (STAT5B, MED1) and histone modification H3K27ac. The reads were shifted 100 bp from their 5′ starts to represent the center of the DNA fragment associated with the reads. For RNA-Seq data, raw counts falling on exons of each gene were calculated and normalized by using RPKM (Reads Per Kilobase per Million mapped reads). Differentially expressed genes were identified with R Bioconductor package “edgeR” (77). RNA-Seq analysis of in vitro-derived control and *Stat5a;Stat5b* DKO DN2 cells was performed as described previously (31).

Super-enhancer analysis was performed using HOMER with settings: -style super -o auto -superSlope −1000 -minDist 15000. In brief, STAT5 peaks that were found within 15 kb of one another were “stretched” together as super-enhancer regions. The signal of each super-enhancer was then determined by the total normalized number reads minus the number of normalized reads in the input (IgG). These regions were then sorted by their score, normalized to the highest score and the number of putative enhancer regions, and then super-enhancers identified as regions past the point where the slope is greater than 1.

Supplementary Material

Refer to Web version on PubMed Central for supplementary material.

Acknowledgments:

We thank Dr. Ning Du for help with mast cell STAT5 ChIP-Seq studies. We thank Dr. Keji Zhao for valuable discussions and critical comments. For ChIP-Seq and RNA-Seq analysis, DNA sequencing was performed in the NHLBI DNA Sequencing Core.

Funding:

This work was supported by the Division of Intramural Research, National Heart, Lung, and Blood Institutes, NHLBI (W.J.L); NIH grants R01AI135200 and R01HD100039 (E.V.R.); R01AI121426 and R01HL114093 (V.P.). B.S. was supported by a Cancer Research Institute-Irvington Postdoctoral Fellowship. S.G., K.S., and K.N. were supported by the Intramural Research Program of NIAMS and the NIAMS Office of Scientific Technology for flow cytometry and sequencing. B.Y was supported by the SIRG Graduate Research Assistantships Award. M.K was supported by the Purdue University Center for Cancer Research P30CA23168.

Data and materials availability:

For the RNA expression in control and *Stat5a;Stat5b* double knockout DN2 cells, the GSE accession number is GSE184845 (https://www.ncbi.nlm.nih.gov/geo/query/acc.cgi?acc=GSE184845). For the RNA-Seq data from IL-2-induced $CD8^+$ T cells (58), the GSE accession number is GSE143903. Other data can be viewed at https://nih.box.com/s/6bmco09put8ilgo1pgqd2xfdfzrrmff9 and raw data will be deposited in GEO database prior to publication. Previously published data were accessed from GSE 110020, 148441, 110305,

218147, and 46662. All materials generated in this study will be made available upon request.

References and Notes

1. Hnisz D et al. , Super-enhancers in the control of cell identity and disease. Cell 155, 934–947 (2013). [PubMed: 24119843]
2. Whyte WA et al. , Master transcription factors and mediator establish super-enhancers at key cell identity genes. Cell 153, 307–319 (2013). [PubMed: 23582322]
3. Hay D et al. , Genetic dissection of the alpha-globin super-enhancer in vivo. Nat Genet 48, 895–903 (2016). [PubMed: 27376235]
4. Pott S, Lieb JD, What are super-enhancers? Nat Genet 47, 8–12 (2015). [PubMed: 25547603]
5. Adam RC et al. , Pioneer factors govern super-enhancer dynamics in stem cell plasticity and lineage choice. Nature 521, 366–370 (2015). [PubMed: 25799994]
6. Chong S et al. , Imaging dynamic and selective low-complexity domain interactions that control gene transcription. Science 361, (2018).
7. Sabari BR et al. , Coactivator condensation at super-enhancers links phase separation and gene control. Science 361, (2018).
8. Rowley MJ, Corces VG, Organizational principles of 3D genome architecture. Nat Rev Genet 19, 789–800 (2018). [PubMed: 30367165]
9. Cross SL et al. , Regulation of the human interleukin-2 receptor alpha chain promoter: activation of a nonfunctional promoter by the transactivator gene of HTLV-I. Cell 49, 47–56 (1987). [PubMed: 3030566]
10. Cross SL, Halden NF, Lenardo MJ, Leonard WJ, Functionally distinct NF-kappa B binding sites in the immunoglobulin kappa and IL-2 receptor alpha chain genes. Science 244, 466–469 (1989). [PubMed: 2497520]
11. John S, Robbins CM, Leonard WJ, An IL-2 response element in the human IL-2 receptor alpha chain promoter is a composite element that binds Stat5, Elf-1, HMG-I(Y) and a GATA family protein. EMBO J 15, 5627–5635 (1996). [PubMed: 8896456]
12. John S et al. , Regulation of cell-type-specific interleukin-2 receptor alpha-chain gene expression: potential role of physical interactions between Elf-1, HMG-I(Y), and NF-kappa B family proteins. Mol Cell Biol 15, 1786–1796 (1995). [PubMed: 7862168]
13. Kim HP, Kelly J, Leonard WJ, The basis for IL-2-induced IL-2 receptor alpha chain gene regulation: importance of two widely separated IL-2 response elements. Immunity 15, 159–172 (2001). [PubMed: 11485747]
14. Kim HP, Leonard WJ, The basis for TCR-mediated regulation of the IL-2 receptor alpha chain gene: role of widely separated regulatory elements. EMBO J 21, 3051–3059 (2002). [PubMed: 12065418]
15. Soldaini E et al. , Mouse interleukin-2 receptor alpha gene expression. Delimitation of cis-acting regulatory elements in transgenic mice and by mapping of DNase-I hypersensitive sites. J Biol Chem 270, 10733–10742 (1995). [PubMed: 7738012]
16. Rameil P et al. , IL-2 and long-term T cell activation induce physical and functional interaction between STAT5 and ETS transcription factors in human T cells. Oncogene 19, 2086–2097 (2000). [PubMed: 10815800]
17. Yeh JH et al. , Control of IL-2Ralpha gene expression: structural changes within the proximal enhancer/core promoter during T-cell development. Nucleic Acids Res 30, 1944–1951 (2002). [PubMed: 11972331]
18. Yeh JH et al. , Novel CD28-responsive enhancer activated by CREB/ATF and AP-1 families in the human interleukin-2 receptor alpha-chain locus. Mol Cell Biol 21, 4515–4527 (2001). [PubMed: 11416131]
19. Kim HP, Imbert J, Leonard WJ, Both integrated and differential regulation of components of the IL-2/IL-2 receptor system. Cytokine Growth Factor Rev 17, 349–366 (2006). [PubMed: 16911870]

20. Liao W, Lin JX, Leonard WJ, Interleukin-2 at the crossroads of effector responses, tolerance, and immunotherapy. Immunity 38, 13–25 (2013). [PubMed: 23352221]
21. Li P et al. , STAT5-mediated chromatin interactions in superenhancers activate IL-2 highly inducible genes: Functional dissection of the Il2ra gene locus. Proc Natl Acad Sci U S A 114, 12111–12119 (2017). [PubMed: 29078395]
22. Simeonov DR et al. , Discovery of stimulation-responsive immune enhancers with CRISPR activation. Nature 549, 111–115 (2017). [PubMed: 28854172]
23. Leonard WJ, Lin JX, O'Shea JJ, The gammac Family of Cytokines: Basic Biology to Therapeutic Ramifications. Immunity 50, 832–850 (2019). [PubMed: 30995502]
24. Rothenberg EV, Moore JE, Yui MA, Launching the T-cell-lineage developmental programme. Nat Rev Immunol 8, 9–21 (2008). [PubMed: 18097446]
25. Yao Z et al. , Stat5a/b are essential for normal lymphoid development and differentiation. Proc Natl Acad Sci U S A 103, 1000–1005 (2006). [PubMed: 16418296]
26. Nakajima H et al. , An indirect effect of Stat5a in IL-2-induced proliferation: a critical role for Stat5a in IL-2-mediated IL-2 receptor alpha chain induction. Immunity 7, 691–701 (1997). [PubMed: 9390692]
27. Imada K et al. , Stat5b is essential for natural killer cell-mediated proliferation and cytolytic activity. J Exp Med 188, 2067–2074 (1998). [PubMed: 9841920]
28. Montel-Hagen A et al. , In Vitro Recapitulation of Murine Thymopoiesis from Single Hematopoietic Stem Cells. Cell Rep 33, 108320 (2020). [PubMed: 33113379]
29. Schmitt TM, Zuniga-Pflucker JC, Induction of T cell development from hematopoietic progenitor cells by delta-like-1 in vitro. Immunity 17, 749–756 (2002). [PubMed: 12479821]
30. Romero-Wolf M et al. , Notch2 complements Notch1 to mediate inductive signaling that initiates early T cell development. J Cell Biol 219, (2020).
31. Shin B et al. , Runx1 and Runx3 drive progenitor to T-lineage transcriptome conversion in mouse T cell commitment via dynamic genomic site switching. Proc Natl Acad Sci U S A 118, (2021).
32. Zhou W et al. , Single-Cell Analysis Reveals Regulatory Gene Expression Dynamics Leading to Lineage Commitment in Early T Cell Development. Cell Syst 9, 321–337 e329 (2019). [PubMed: 31629685]
33. Chen ELY, Thompson PK, Zuniga-Pflucker JC, RBPJ-dependent Notch signaling initiates the T cell program in a subset of thymus-seeding progenitors. Nat Immunol 20, 1456–1468 (2019). [PubMed: 31636466]
34. Liu H et al. , Notch dimerization is required for leukemogenesis and T-cell development. Genes Dev 24, 2395–2407 (2010). [PubMed: 20935071]
35. Del Real MM, Rothenberg EV, Architecture of a lymphomyeloid developmental switch controlled by PU.1, Notch and Gata3. Development 140, 1207–1219 (2013). [PubMed: 23444353]
36. Guo Y, Maillard I, Chakraborti S, Rothenberg EV, Speck NA, Core binding factors are necessary for natural killer cell development and cooperate with Notch signaling during T-cell specification. Blood 112, 480–492 (2008). [PubMed: 18390836]
37. Liu P, Li P, Burke S, Critical roles of Bcl11b in T-cell development and maintenance of T-cell identity. Immunol Rev 238, 138–149 (2010). [PubMed: 20969590]
38. Weber BN et al. , A critical role for TCF-1 in T-lineage specification and differentiation. Nature 476, 63–68 (2011). [PubMed: 21814277]
39. Yoshida H et al. , The cis-Regulatory Atlas of the Mouse Immune System. Cell 176, 897–912 e820 (2019). [PubMed: 30686579]
40. Hosokawa H, Rothenberg EV, Cytokines, Transcription Factors, and the Initiation of T-Cell Development. Cold Spring Harb Perspect Biol 10, (2018).
41. Anderson MK, Weiss AH, Hernandez-Hoyos G, Dionne CJ, Rothenberg EV, Constitutive expression of PU.1 in fetal hematopoietic progenitors blocks T cell development at the pro-T cell stage. Immunity 16, 285–296 (2002). [PubMed: 11869688]
42. Dionne CJ et al. , Subversion of T lineage commitment by PU.1 in a clonal cell line system. Dev Biol 280, 448–466 (2005). [PubMed: 15882585]

43. Cheng G, Yu A, Dee MJ, Malek TR, IL-2R signaling is essential for functional maturation of regulatory T cells during thymic development. J Immunol 190, 1567–1575 (2013). [PubMed: 23315074]
44. Owen DL et al. , Identification of Cellular Sources of IL-2 Needed for Regulatory T Cell Development and Homeostasis. J Immunol 200, 3926–3933 (2018). [PubMed: 29728511]
45. Owen DL et al. , Thymic regulatory T cells arise via two distinct developmental programs. Nat Immunol 20, 195–205 (2019). [PubMed: 30643267]
46. Dikiy S et al. , A distal Foxp3 enhancer enables interleukin-2 dependent thymic Treg cell lineage commitment for robust immune tolerance. Immunity 54, 931–946 e911 (2021). [PubMed: 33838102]
47. Smith GA, Taunton J, Weiss A, IL-2Rbeta abundance differentially tunes IL-2 signaling dynamics in CD4(+) and CD8(+) T cells. Sci Signal 10, (2017).
48. Kim HP, Kim BG, Letterio J, Leonard WJ, Smad-dependent cooperative regulation of interleukin 2 receptor alpha chain gene expression by T cell receptor and transforming growth factor-beta. J Biol Chem 280, 34042–34047 (2005). [PubMed: 16087671]
49. Zhang S et al. , Reversing SKI-SMAD4-mediated suppression is essential for TH17 cell differentiation. Nature 551, 105–109 (2017). [PubMed: 29072299]
50. Di Santo JP, Natural killer cell developmental pathways: a question of balance. Annu Rev Immunol 24, 257–286 (2006). [PubMed: 16551250]
51. Lin JX et al. , Critical functions for STAT5 tetramers in the maturation and survival of natural killer cells. Nat Commun 8, 1320 (2017). [PubMed: 29105654]
52. Lee SH, Fragoso MF, Biron CA, Cutting edge: a novel mechanism bridging innate and adaptive immunity: IL-12 induction of CD25 to form high-affinity IL-2 receptors on NK cells. J Immunol 189, 2712–2716 (2012). [PubMed: 22888135]
53. Toomer KH et al. , Essential and non-overlapping IL-2Ralpha-dependent processes for thymic development and peripheral homeostasis of regulatory T cells. Nat Commun 10, 1037 (2019). [PubMed: 30833563]
54. Betz RC et al. , Genome-wide meta-analysis in alopecia areata resolves HLA associations and reveals two new susceptibility loci. Nat Commun 6, 5966 (2015). [PubMed: 25608926]
55. Xing L et al. , Alopecia areata is driven by cytotoxic T lymphocytes and is reversed by JAK inhibition. Nat Med 20, 1043–1049 (2014). [PubMed: 25129481]
56. Scharschmidt TC et al. , A Wave of Regulatory T Cells into Neonatal Skin Mediates Tolerance to Commensal Microbes. Immunity 43, 1011–1021 (2015). [PubMed: 26588783]
57. Creyghton MP et al. , Histone H3K27ac separates active from poised enhancers and predicts developmental state. Proc Natl Acad Sci U S A 107, 21931–21936 (2010). [PubMed: 21106759]
58. Hermans D et al. , Lactate dehydrogenase inhibition synergizes with IL-21 to promote CD8(+) T cell stemness and antitumor immunity. Proc Natl Acad Sci U S A 117, 6047–6055 (2020). [PubMed: 32123114]
59. Kagey MH et al. , Mediator and cohesin connect gene expression and chromatin architecture. Nature 467, 430–435 (2010). [PubMed: 20720539]
60. Radtke F, MacDonald HR, Tacchini-Cottier F, Regulation of innate and adaptive immunity by Notch. Nat Rev Immunol 13, 427–437 (2013). [PubMed: 23665520]
61. Adler SH et al. , Notch signaling augments T cell responsiveness by enhancing CD25 expression. J Immunol 171, 2896–2903 (2003). [PubMed: 12960312]
62. Borcherding N et al. , A transcriptomic map of murine and human alopecia areata. JCI Insight 5, (2020).
63. Samstein RM et al. , Foxp3 exploits a pre-existent enhancer landscape for regulatory T cell lineage specification. Cell 151, 153–166 (2012). [PubMed: 23021222]
64. Bahr C et al. , A Myc enhancer cluster regulates normal and leukaemic haematopoietic stem cell hierarchies. Nature 553, 515–520 (2018). [PubMed: 29342133]
65. Herranz D et al. , A NOTCH1-driven MYC enhancer promotes T cell development, transformation and acute lymphoblastic leukemia. Nat Med 20, 1130–1137 (2014). [PubMed: 25194570]

66. Kieffer-Kwon KR et al. , Interactome maps of mouse gene regulatory domains reveal basic principles of transcriptional regulation. Cell 155, 1507–1520 (2013). [PubMed: 24360274]

67. Fujioka M, Emi-Sarker Y, Yusibova GL, Goto T, Jaynes JB, Analysis of an even-skipped rescue transgene reveals both composite and discrete neuronal and early blastoderm enhancers, and multi-stripe positioning by gap gene repressor gradients. Development 126, 2527–2538 (1999). [PubMed: 10226011]

68. Small S, Arnosti DN, Levine M, Spacing ensures autonomous expression of different stripe enhancers in the even-skipped promoter. Development 119, 762–772 (1993). [PubMed: 8187640]

69. Shin HY et al. , Hierarchy within the mammary STAT5-driven Wap super-enhancer. Nat Genet 48, 904–911 (2016). [PubMed: 27376239]

70. Huang J et al. , Dissecting super-enhancer hierarchy based on chromatin interactions. Nat Commun 9, 943 (2018). [PubMed: 29507293]

71. Zamudio AV et al. , Mediator Condensates Localize Signaling Factors to Key Cell Identity Genes. Mol Cell 76, 753–766 e756 (2019). [PubMed: 31563432]

72. Butler A, Hoffman P, Smibert P, Papalexi E, Satija R, Integrating single-cell transcriptomic data across different conditions, technologies, and species. Nat Biotechnol 36, 411–420 (2018). [PubMed: 29608179]

73. Lin JX et al. , Critical Role of STAT5 transcription factor tetramerization for cytokine responses and normal immune function. Immunity 36, 586–599 (2012). [PubMed: 22520852]

74. Langmead B, Trapnell C, Pop M, Salzberg SL, Ultrafast and memory-efficient alignment of short DNA sequences to the human genome. Genome Biol 10, R25 (2009). [PubMed: 19261174]

75. Trapnell C, Pachter L, Salzberg SL, TopHat: discovering splice junctions with RNA-Seq. Bioinformatics 25, 1105–1111 (2009). [PubMed: 19289445]

76. Robinson JT et al. , Integrative genomics viewer. Nat Biotechnol 29, 24–26 (2011). [PubMed: 21221095]

77. Robinson MD, McCarthy DJ, Smyth GK, edgeR: a Bioconductor package for differential expression analysis of digital gene expression data. Bioinformatics 26, 139–140 (2010). [PubMed: 19910308]

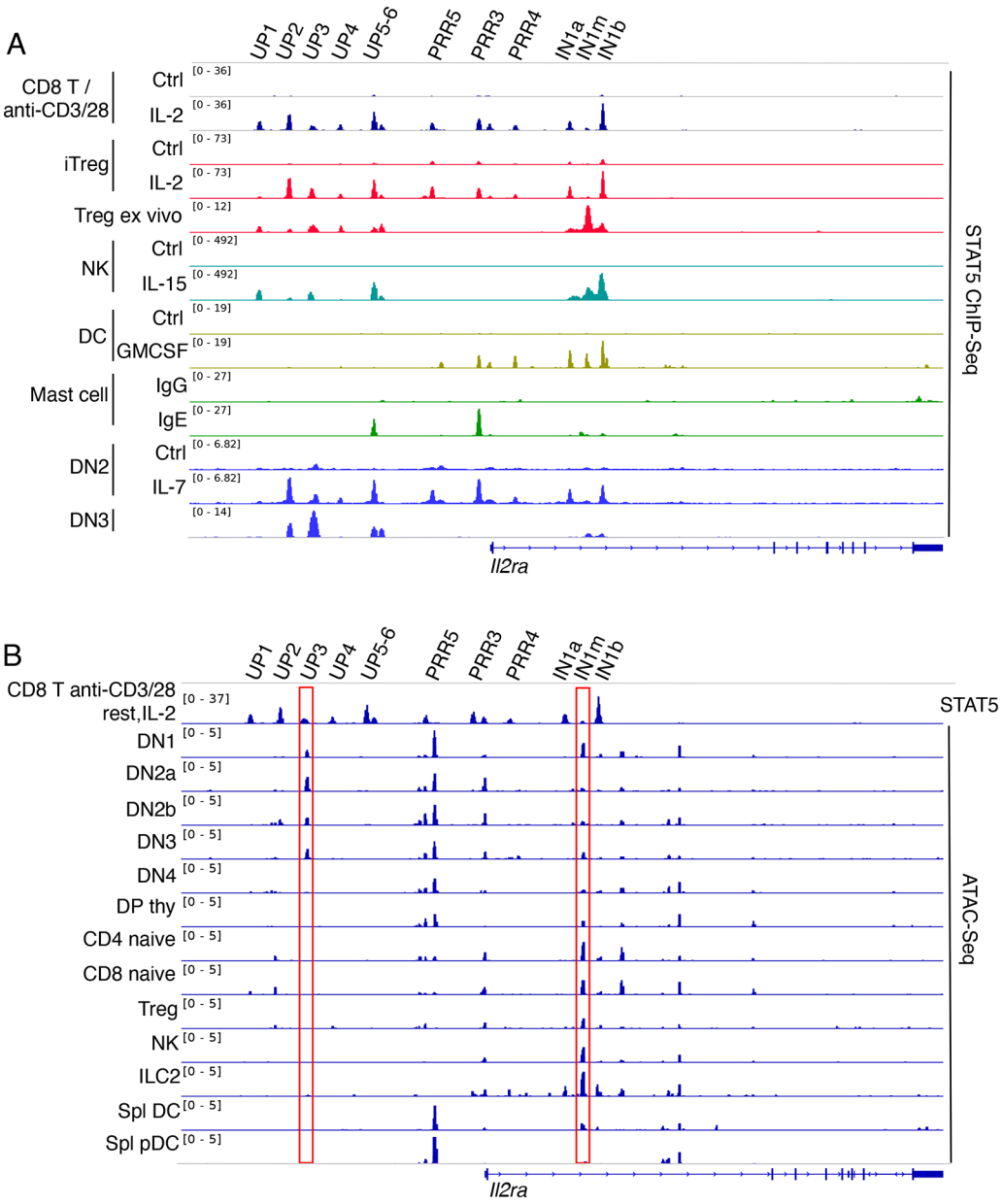

Fig. 1.

Lineage and developmental chromatin structure at the *Il2ra* super-enhancer. **(A)** STAT5 binding as assessed by ChIP-Seq experiments using *in vitro* activated lymphoid ($CD8^+$ T cells, iTreg cells, NK cells, and DN2 thymocytes) and myeloid populations (splenic DCs and mast cells) or *ex vivo* populations (DN3 and Treg cells). The $CD8^+$ T cells were pre-activated with anti-CD3 + CD28 for 2 days, rested for 4 h, and then not stimulated or stimulated with IL-2 for 4 h. All ChIP-Seq experiments were performed on two independent samples, with similar results. Representative data are shown. **(B)** Open chromatin regions in the *Il2ra* locus as assessed by ATAC-Seq. Red rectangles highlight regions that appear to be developmentally significant. Data are from the ImmGen database.

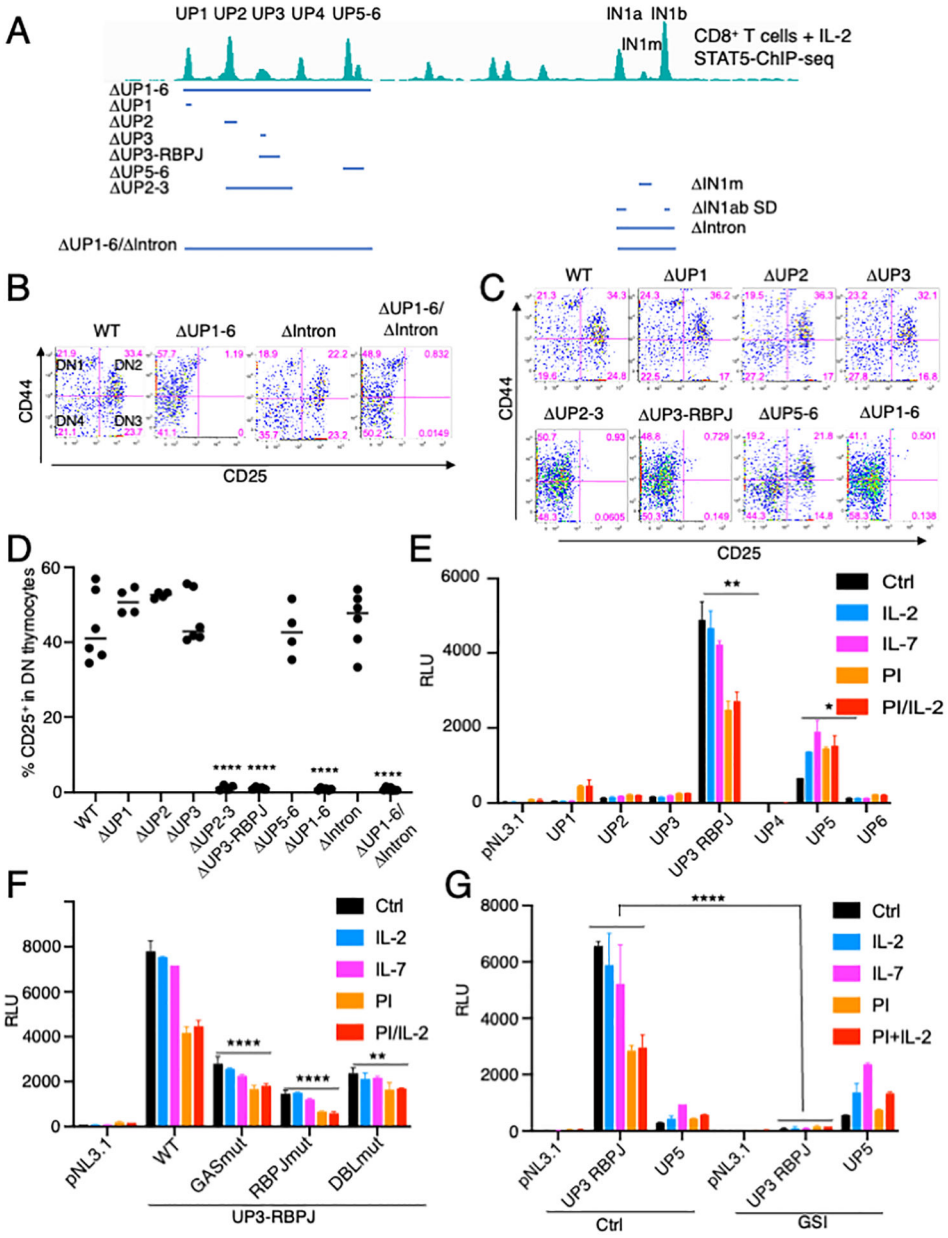

Fig. 2.

Upstream enhancer elements control constitutive CD25 expression in DN thymocytes. **(A)** Schematic summary of CRISPR-Cas9 generated mutant mice, compared with STAT5B ChIP-seq binding data from stimulated $CD8^+$ T cells. Indicated are the upstream or intronic regions that were deleted; these mutants were used to determine the functional importance of individual or groups of elements within the *Il2ra* super-enhancer. **(B)** Flow cytometry profiles gated on $CD4^-CD8^-$ double negative thymocytes from mice containing either the UP1–6 upstream deletion (ΔUP1–6), the intron deletion (Δintron), or deletion of both regions. The data are representative of 3 experiments. **(C and D)** Representative flow cytometry data of DN thymocytes from the indicated mutant mice (**C**), with data from multiple (two to three) experiments summarized in **(D)**. Shown is the percentage of

DN cells that express CD25 (i.e., DN2 + DN3 cells). Differences were compared to WT mice using Student's t-test (n=4–6, ****p<0.0001). **(E)** *In vitro* transfection of a DN3 cell line (SCID.Adh.2C2), with individual upstream (UP) regions cloned into pNL3.1 reporter construct. **(F)** A WT UP3/RBPJ reporter construct or reporters containing mutation of the GAS motif, the RBPJ motif, or both motifs were transfected into the DN3 cell line. **(G)** Treatment of the cells with a γ-secretase inhibitor to block Notch signaling reduced reporter expression by the UP3/RBPJ construct but did not block expression from a UP5 reporter construct. **E-G** are representative of 3 experiments, and reporter activities in all treatment groups were compared to those in either the empty vector (**E**) or to the WT construct (**F**) or to the control group (**G**) using Student's t-test (n=3, *p<0.05, **p<0.001, ****p<0.0001).

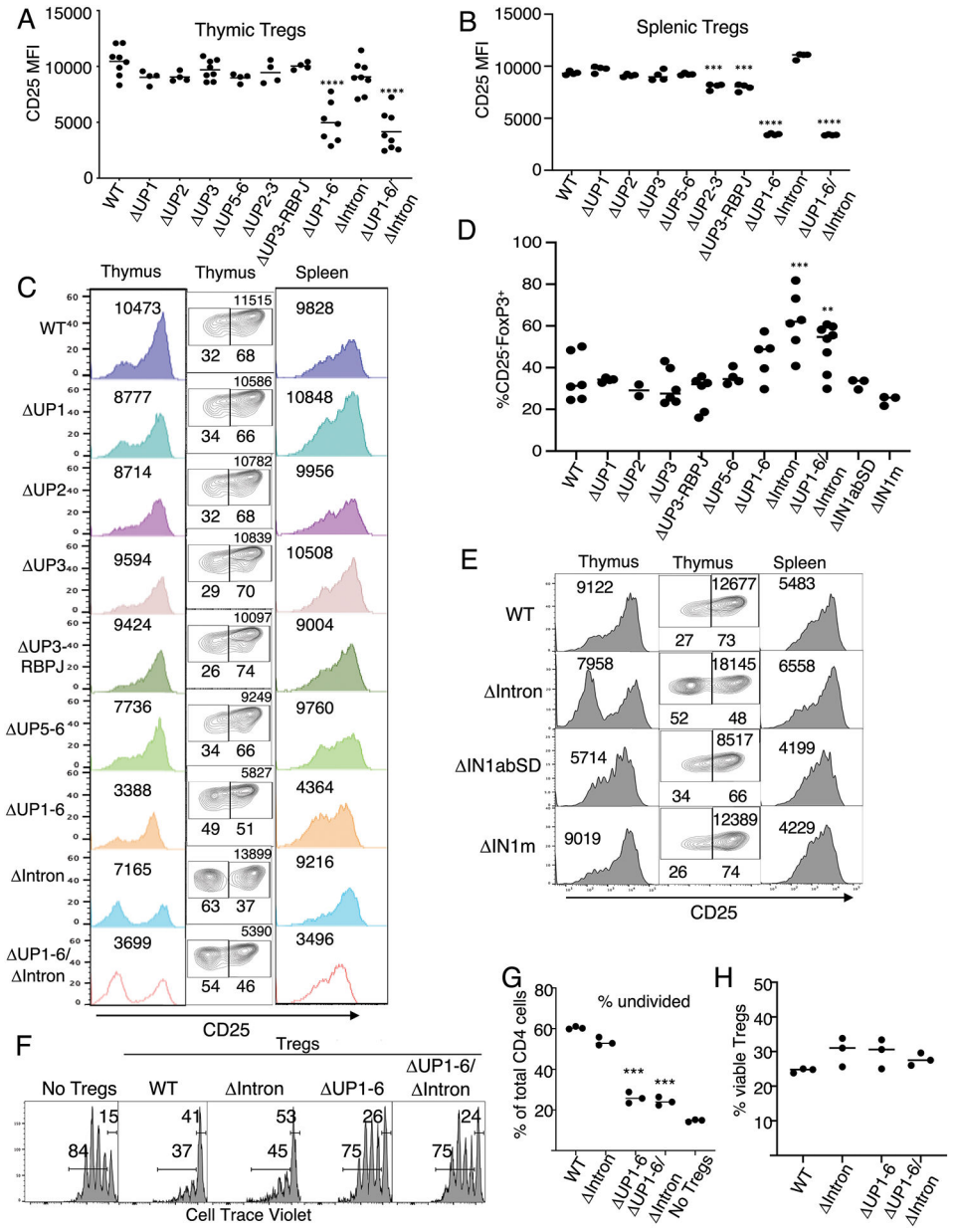

Fig. 3.

Upstream enhancer elements control the level of constitutive CD25 expression in both thymic and splenic Treg cells. **(A to C)** Flow cytometry profiles for CD25 expression (MFI) gated on $CD4^{+}FoxP3^{+}$ thymic and splenic cells from mice with upstream and intronic deletions in the *Il2ra* super-enhancer. Data for thymic Tregs (**A**) and splenic Tregs (**B**) were combined from two to three experiments with one representative experiment in **(C)** showing the histograms of thymic Tregs on the left and splenic Tregs on the right panel. In **C**, the middle panel gates on the $CD25^{low}$ and $CD25^{hi}$ thymic Tregs; the percentages of the $CD25^{low}$ and $CD25^{hi}$ thymic Tregs are indicated as is the MFI of the latter population. (**D**) Summary (from 2–3 experiments) of the percentage of $CD25^{low}$ cells within the thymic $FoxP3^{+}$ population of mice with deletions of upstream or intronic enhancer regions. (**E**)

Representative profiles from intron deletion mutants of thymic Tregs (left panel) and splenic Tregs (right panel), with the middle panel gating on $CD25^{low}$ and $CD25^{hi}$ thymic Tregs; the percentages of these are indicated as well as the MFI of the latter population. **(F and G)** Splenic Treg suppressive activity as measured by inhibition of WT $CD4^+$ T cell proliferation (see Methods). Cell Trace Violet dilution at day 3 $CD4^+$ T cells co-cultured with purified splenic Tregs from WT, ΔIntron, ΔUP1–6 or ΔUP1–6/ΔIntron mice; shown are a representative experiment (**F**) and the % undivided cells from 3 mice (**G**). (**H**) Viability of Tregs at the end of the suppression assay, as assessed by flow cytometry. Differences in MFI or population percentages compared to WT were compared using Student's t-test (n=3–8, *p<0.05, **p<0.01, ***p<0.001, ****p<0.0001).

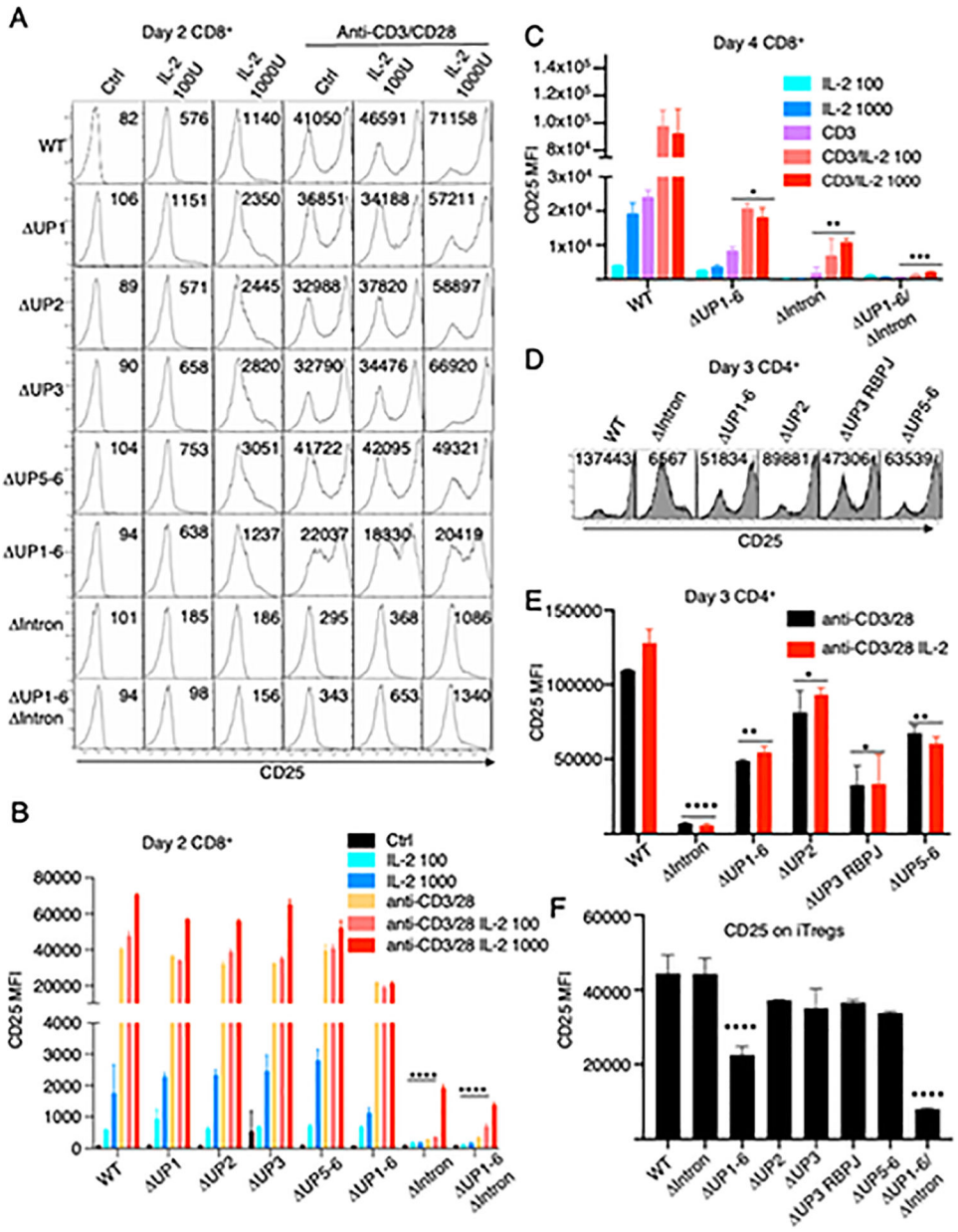

Fig. 4.

Inducible CD25 expression in CD8$^+$ and CD4$^+$ T cells is strongly regulated by intronic enhancer elements. **(A and B)** Flow cytometric measurement of CD25 surface expression on CD8$^+$ T cells isolated from WT or the indicated mutant mice and stimulated with or without IL-2 in the presence or absence of anti-CD3 + anti-CD28. Representative histograms at day 2 are shown in **(A)** with collective MFI data from 2 experiments depicted in **(B)**. (**C**) Summary of flow cytometric measurement of CD25 surface expression on CD8$^+$ T cells isolated from WT or the indicated mutant mice and stimulated with or without IL-2 in the absence or presence of anti-CD3 + anti-CD28. Analysis was performed at day 4. **(D and E)** CD4$^+$ T cells isolated from WT or from the indicated mice were activated with anti-CD3 + anti-CD28 in the presence of IL-2 for 3 days, and CD25 expression was measured by flow

cytometry. Representative profiles are shown in **(D)**, and collective profiles are shown in **(E)**. **(F)** Naïve $CD4^+$ T cells from the indicated mice were activated under iTreg conditions with TGFβ + IL-2 + anti-IFNγ and anti-IL-4 for 3 days. CD25 expression was then measured by flow cytometry. **A**-**F** are representative of 3 independent experiments. In all panels, MFI values for stimulated cells in mutant mice were compared to corresponding cells in WT mice by Student's t-test (n=3 *p<0.05, **p<0.01, ***p<0.001, ****p<0.0001).

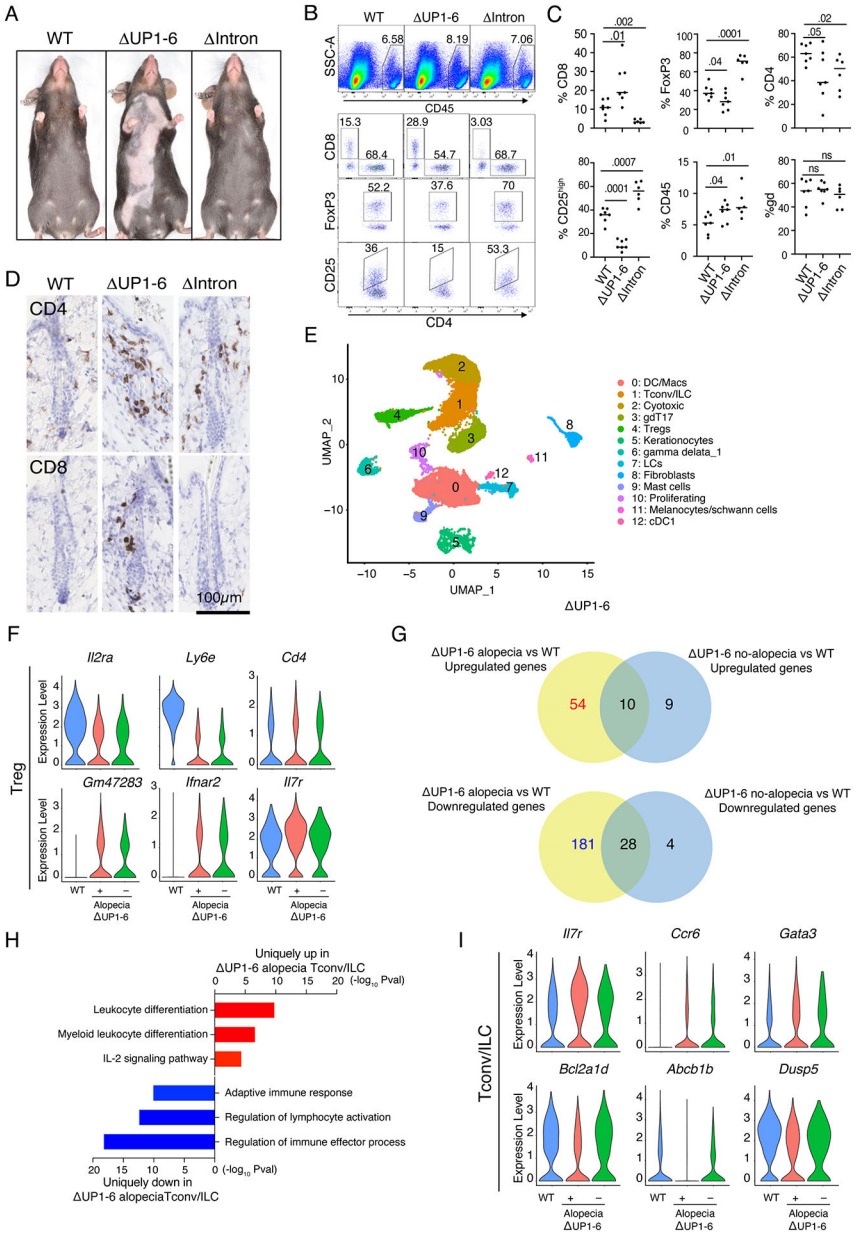

Fig. 5. Deletion of the upstream enhancer region leads to spontaneous autoimmune alopecia.

(A) Representative pictures of hair loss in ΔUP1–6 mice compared to WT or ΔIntron mice. **(B)** Representative flow cytometric profiles of skin lymphoid populations. (**C**) Collective profiles of cellular populations from 2 independent experiments. Percentages of populations were compared to WT using Student's t-test (n=6–7, p-values are shown). **(D)** Immunohistochemistry of skin from WT, ΔUP1–6, or ΔIntron mice stained for CD4 and CD8 expression. See Methods for the antibodies that were used. **(E)** Clustering of immune populations in CD45+ skin using Seurat clustering. **(F)** Differentially expressed genes in Tregs of WT vs ΔUP1–6 alopecia or non-alopecia skin. **(G)** Venn diagram illustrating differentially expressed genes in WT vs ΔUP1–6 alopecia vs non-alopecia skin. **(H)** Metascape pathway analysis of differentially expressed genes either upregulated or

downregulated in in Tconv/ILC skin populations in ΔUP1–6 mice with alopecia. **(I)** Genes uniquely up- or down-regulated in Tconv/ILC skin populations ΔUP1–6 mice with alopecia.

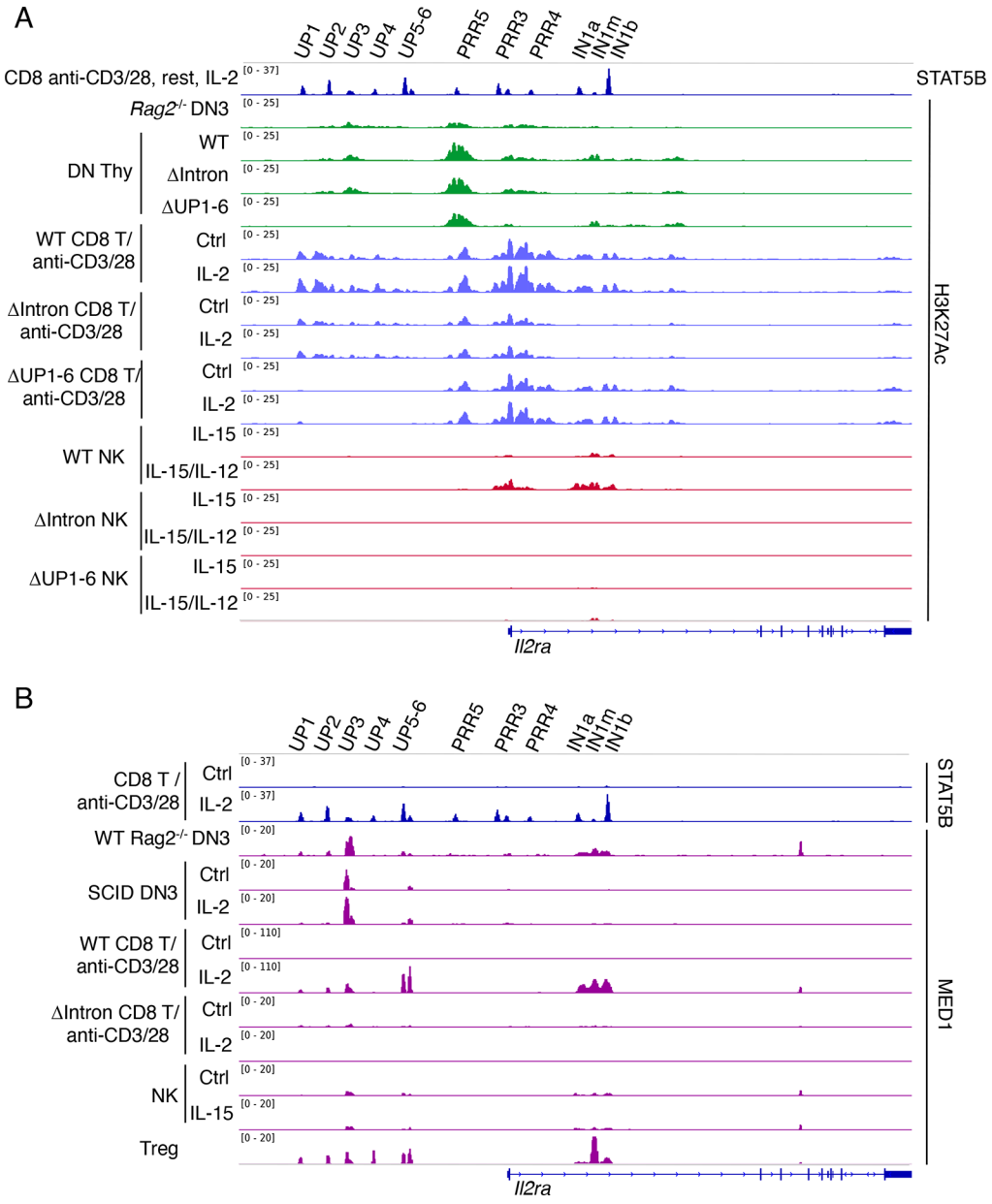

Fig. 6.

Super-enhancer structure is distinct at different developmental stages. **(A)** ChIP-Seq profiles for H3K27Ac marks were assessed in *ex vivo* isolated *Rag2*$^{-/-}$ DN3 thymocytes, DN thymocytes from WT, ΔIntron and ΔUP1–6 mice; in WT, ΔIntron and ΔUP1–6 CD8^{+} T cells that were stimulated in vitro with anti-CD3 + anti-CD28 without or with 1000 U IL-2 for 48 hrs; and in NK cells that were stimulated with IL-15 or IL-15 + IL-12. **(B)** ChIP-Seq profiles for MED1 were assayed in DN3 thymic cells, in vitro activated CD8^{+} T cells and NK cells, and *ex vivo* Treg cells. All ChIP-Seq results are representative of two independent experiments. All ChIP-Seq experiments in **A** and **B** were performed on two independent samples, with similar results. Representative data are shown.

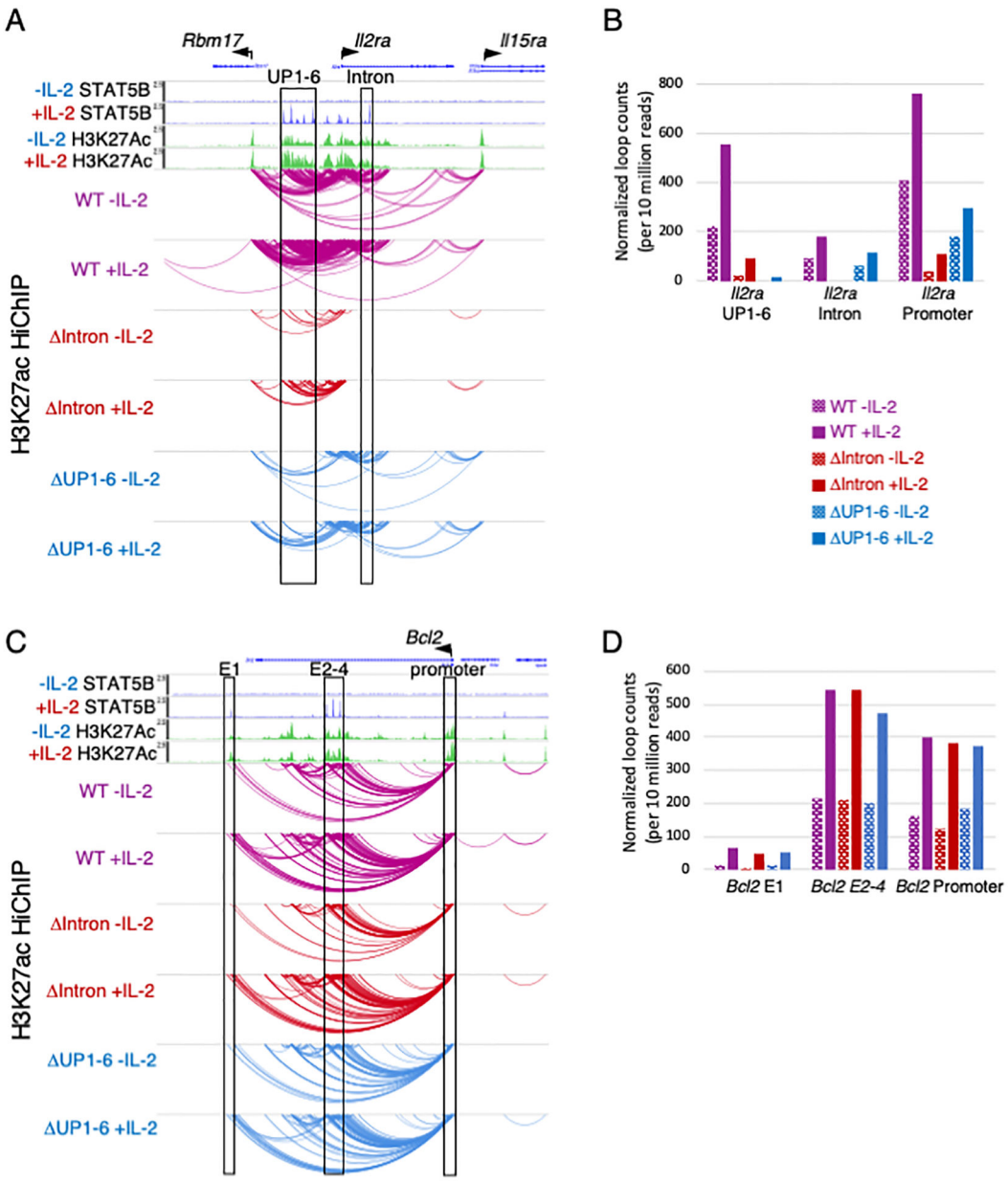

Fig. 7.

Higher order chromatin looping within the *Il2ra* super-enhancer is disrupted by the loss of the intronic region. H3K27Ac HiChIP assay showing chromatin interactions at the *Il2ra* **(A and B)** and *Bcl2* **(C and D)** loci in $CD8^+$ T cells from WT, ΔIntron, or ΔUP1–6 mice that were activated with anti-CD3 + anti-CD28 and then not stimulated or stimulated with IL-2. H3K27Ac HiChIP results are representative of two independent experiments.